A magnetotelluric investigation in the North German Basin

Case History
by
Nils Feyerabend

Mai 2000

metronix

Metronix Braunschweig

Contents

Coverage of Case History

This case history is supposed to give a review on the magnetotelluric method and to report on the data acquisition of this survey. These data are to be discussed and basicly interpreted. An optimized fitting-technique, considering the TE-mode as suggested by Weidelt, is supposed to be implemented and is to be applied on the data.

The data was acquired with Metronix new 24bit geophysical equipment **ADU06**. Due to the absence of any analogue filters it was possible to obtain data in an area where man made noise makes it almost impossible to record electromagetic fields.

Introduction

The magnetotelluric method, proposed by Cagniard in 1953, belongs to the family of electromagnetic deep sounding methods. The common purpose of electromagnetic deep sounding methods is a prediction of the subsurface electric conductivity.

The magnetotelluric sounding method will be described in Chapter **??**. We will see that the magnetotelluric method is controlled by a diffusive induction process, a process similar to the conduction of heat. The magnetotelluric method determines the ratio of two orthogonal horizontal components of electric and magnetic fields. This ratio, the so-called response or transfer function, is a function of frequency which is determined from measured data.

A measuring equipment for magnetotelluric sounding, provided by Metronix, Braunschweig, will be described in Chapter 1. Since sensors and even the data logger have an influence on the measured time series, frequency characteristics have also to be taken into account.

Chapter 2 reports on a survey in Northern Germany in 1999. This survey has been carried out by **Metroni**x for the Federal Institute of Geosciences and Natural Resources ('Bundesanstalt für Geowissenschaften und Rohstoffe' (BGR)). The acquired data have been processed by a remote reference method with a code provided by Jim Larsen (PMEL, Seattle). The results have been interpreted by a heuristic $\rho^* - z^*$-transformation in first place. An 1D-model interpretation has been applied for the upper frequencies

Chapter **??** reports on an attempt to improve the best fit for the D^+-model by implementing an expansion of the magnetic field presentation. The acquired data of the survey serves as a data pool for numerical experiments of this concept.

Notation

In the sequel vectors of physical fields $\in R^3$ will be written usually in bold face. All field variables in time domain will be denoted in lower case letters (**e**, **b**, etc.) and in frequency domain by capitals (**E**, **B**, etc.). N-Dimensional data vectors and matrices will be written in underlined notation. I refer to Table 1 for the symbols used. The SI system is adopted throughout.

Symbol	Unit	Meaning
$\mathbf{E}$	V/m	electric field
$\mathbf{D}$	As/m^2	electric flux
$\mathbf{B}$	nT	magnetic flux
$\mathbf{H}$	A/m	magnetic field
ϵ_0	$8.8542 \cdot 10^{-12} As/Vm$	electric permittivity
μ_0	$4\pi \cdot 10^{-7} Vs/Am$	magnetic permeability
ρ	Ωm	resistivity
σ	S/m	conductivity
τ	S	conductance
S	S	cumulative conductance
Z_{ij}	m/s	magnetotelluric impedance
C_{ij}	m	complex penetration depth

Symbol	Meaning
a^*	complex conjugate of a
$\underline{\underline{\mathbf{A}}}^+$	adjoint of matrix $\underline{\underline{\mathbf{A}}}$

Table 1: Symbols used in SI system

Chapter 1

Equipment GMS 06

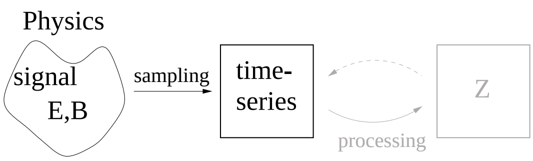

A magnetotelluric equipment measures the horizontal electric and all magnetic field components. The sensors are realized by electrodes and induction coils. The heart of a measuring equipment is the datalogger for signal recording. Therefore a single site setup consists of at least

- a datalogger (ADU06)
- three coils (MFS05 or MFS06)
- four electrodes (EFP 05).

The latest magnetotelluric measuring equipment offered by **Metronix** is the **G**eophysical **M**easuring **S**ystem GMS 06. Its individual components and their characteristics will be described in the following sections.

1.1 Datalogger ADU-06

The latest datalogger built by **Metronix** is the ADU-06. It is the result of a development of a series of previous dataloggers. Important for this kind of measuring instrument is its long time stability concerning time accuracy and outdoor influences like variable temperature, moisture, etc. Finally an exact synchronous recording of five input channels for all field components has to be granted.

1.1.1 General properties

The datalogger ADU-06 (**A**nalog **D**igital **U**nit) is built for exact synchronous multi-channel measurements. This is necessary for the magnetotelluric method, since the phase between these signals contains important information. The unit

Figure 1.1: The datalogger ADU-06 of Metronix, Braunschweig

contains five A/D-boards for recording the signals of two pairs of r electrodes and three magnetometers in a frequency range from DC up to 1 kHz. A 24 Bit sampling resolution allows a wide dynamic signal range. This is necessary in areas with high artificial noise, where records are overmodulated easily.

A GPS-board realizes an exact time base. This is especially important for measurements in a remote reference setup, when synchronous data is processed.

The computer board is based on a 386 CPU for low power consumption of only 7 W to 12 W depending on the measuring configuration.

A network board realizes controlling and downloading of data via laptop. A flash-disk reduces mechanical activity and therefore the number of disturbing parts. A storage capacity of 100 MB allows data recording for long off-line measurements.

The features are summed up in Table 1.1 as an excerpt of the datasheet.

Frequency range	DC to 20 kHz
A/D conversion	24 Bit
System computer	386 based
storage media	Flash-disk 100MB
Network	standard coaxial
Synchronization	GPS clock ±130 ns to satellite reference
Power Consumption	7W-12W
Operating temperature range	-40°C to +70°C

Table 1.1: Features of the datalogger ADU-06 of Metronix, Braunschweig

1.1.2 Controlling

The survey is managed by the provided software MAPROS, which is an enhanced database for survey management with additional abilities of controlling the measuring equipment and single-site processing.

The system is controlled by a graphical user interface. There are several predefined measuring configurations with a corresponding sample frequency F_s [Hz] as summed up in Table 1.2 . The time series are downloaded after each mea-

ADU06 Band	Board	F_s [Hz]	Suffix	Source of excitation	Remark
HF	HF	20 k	a		
LF1	LF	1024	b		
LF2	LF	64	c	pc1	dead band
LF3	LF	2	d	pc1-3, pi1-2	
LF4	LF	0.032	e	pc3-5, pi2	
Free	LF	any	f		

Table 1.2: Typical predefined band conventions of the ADU 06. Last columns remark its typical sources of excitation

suring run, at the end of each measurement. The individual time series files are named by following convention:

ssscrrtb.ats	
sss	ADU06 serial number (001..999)
c	ADU06 channel number (A=1..H=8)
rr	run number (01..99)
t	channel type (a=Ex,b=Ey,x=Hx,y=Hy,z=Hz)
b	band indices

These files contain the data binarily coded. Its format is described in the manual of the datalogger.

1.1.3 Calibration properties

Each A/D-board contains two A/D sampling circuits. One circuit is designed for AMT measurements (HF band) and the other for MT measurements (LF bands LF 1-4). The input characteristics are determined by a cascade of input filters.

Since the following MT measurements are in the low frequency range only the properties of the LF-board are considered. Figure 1.2 shows an example of measured and theoretical phases of the transfer functions for the different type channels. In the range from DC up to 1 kHz the different channels are described by almost the same transfer function. The amplitude is nearly independent of frequency in the given frequency range. Therefore the transfer function needs not to be considered when forming amplitude ratios. For measurements of signals higher than about 3 kHz the transfer function has to be taken into account.

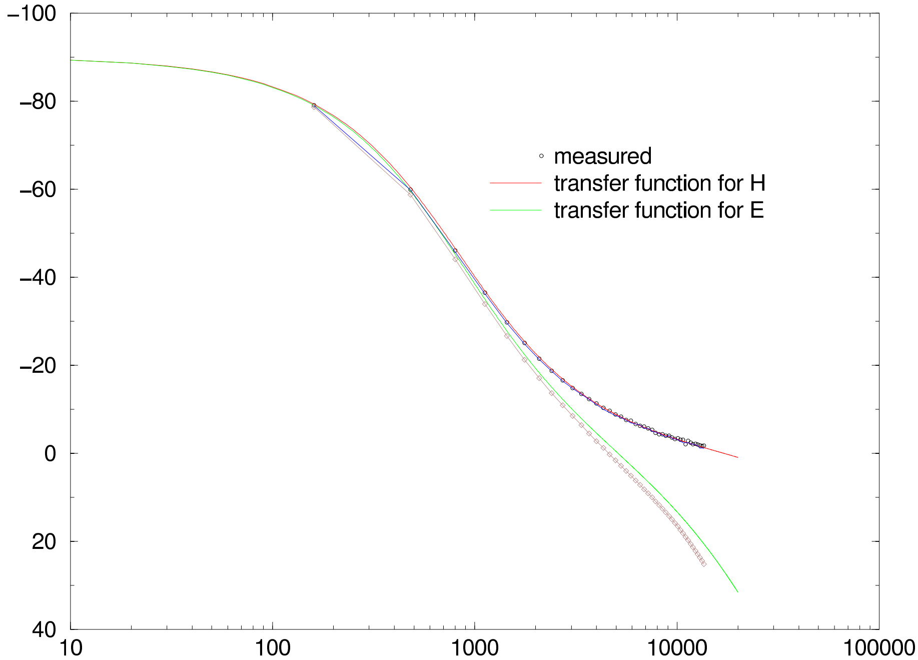

Figure 1.2: Phase [deg] of the transfer function of a ADU-06 A/D-sampling boards versus frequency f [Hz] (Courtesy of Metronix)

1.2 The sensors

The sensors measure the physical field components and provide a voltage signal for recording. Long time stability is required concerning outdoor influences as temperature, moisture, etc. The electrodes measure the electric potential difference at the surface. The induction coils measure the time derivative of the magnetic field.

1.2.1 Electrodes EFP 05

The electrodes EFP 05 are provided by **Metronix**. They are realized by a salt body with a greater surface for low contact resistivity. The information of the datasheet are summarized up in Table 1.3. The temperature drift has been measured in the laboratory of the ELTE University in Budapest (direct correspondence with **Metronix**) turns out to be

$$E[mV] = m \cdot T[^\circ C] + b, \quad m = 0,656,\, b = 534,863.$$

The temperature drift will not be taken into account, since its dominant 24h-period is much longer than the longest time segments used (about 2.5 h).

A transfer function of the electrodes will not be taken into account. The longest measuring runs lasted about four days. The electrodes are supposed to be stable for these periods.

	Long (small)	Medium (normal)
Mass	0.7 kg	1 kg
Diameter	64 mm	90 mm
Height	117 mm	80 mm
Contact Resistance	50-500 Ω	30-300 Ω
Effective surface	27 cm^2	58 cm^2
DC potential	a few mV	a few mV
temperature range	5-50 C	5-50 C
temperature drift	0.66mV/C	0.66mV/C

Table 1.3: Information of the datasheet for the electrodes EFP 05

1.2.2 Induction coil magnetometer MFS-05

The latest induction coil magnetometer provided by **Metronix** is the MFS-05. The MFS-05 consists of an internal amplifier and an induction coil with a high

Figure 1.3: Broadband induction coil MFS 05 built by Metronix, Braunschweig

permeable ferrite core with a great number of copper turns. The induction coil sensor measures the magnetic field's time derivate, expressed by the induction law

$$U_{ind} = -n\frac{d\Phi}{dt}.$$

Here is U_{ind} the induced voltage and n the number of turns of wire. The magnetic flux Φ can be simplified by

$$\Phi = \int_A BdA = BA.$$

or in the frequency domain

$$U_{ind}(\omega) = -i\omega nBA.$$

In addition, the amplifier consists of a number of filters, and a chopper for low frequencies. Therefore the transfer functions are measured individually. These are calibrated in Magnetsrode, TU Braunschweig, by a Solartron spectrum analyzer. Figure 1.4 presents a typical transfer function as delivered with the induction coil by a calibration file.

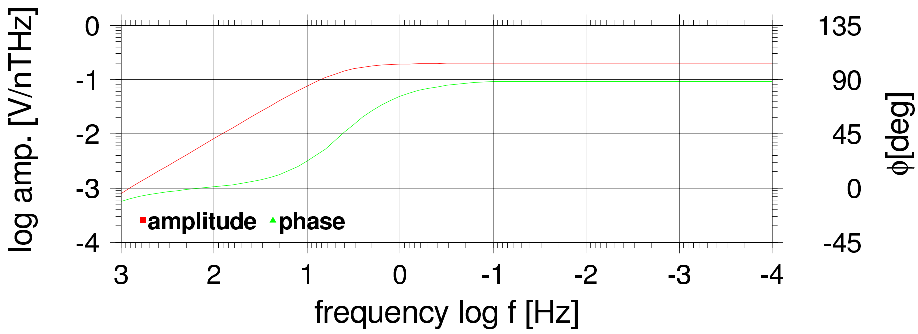

Figure 1.4: Transfer function for a MFS 05 broadband induction coil magnetometer

The MFS-05 behaves like an ideal coil up to about 1 Hz. At higher frequencies eddy currents dominate the curve. The phase also changes from 90 degrees to zero degrees. At a few hundred Hz a high pass will take effect and draws the phase angle down another 180 degrees. The induction coil is specified for a range from 4000 s up to 8 kHz.

1.3 Setting up a magnetotelluric site

A magnetotelluric site is supposed to be placed in an electromagnetically noise-free area. The basic setup configuration is displayed in Figure 1.5.

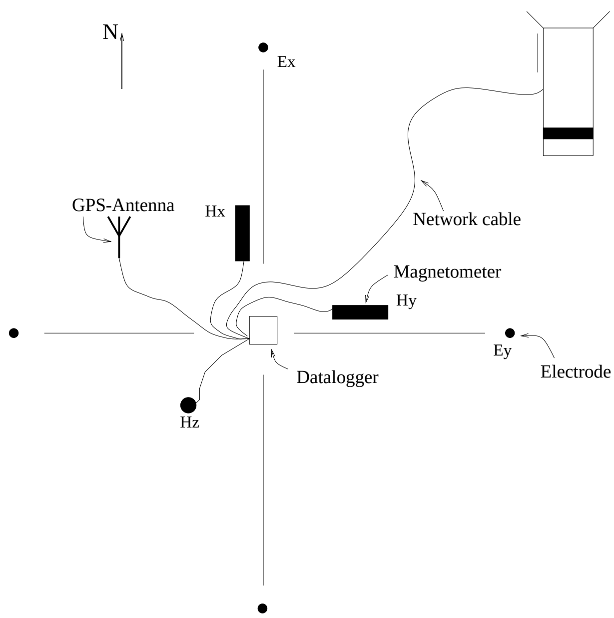

Figure 1.5: Sketch of a basic single site setup

The electrodes are set up in every direction at a distance of 40 meters. The contact resistance has to be checked using a digital voltmeter. This resistance is supposed to be in range of 1 to 10 kΩ depending on the type of soil. It might be necessary to moisten the electrodes in case the salt of the electrodes has been dried out.

The GPS antenna has to be connected for a correct time base and a continuous synchronization for time stability. This is especially necessary for a remote reference setup, when several magnetotelluric sounding stations are measuring synchronously at different sites.

First the magnetometers have to be placed in a parallel position, at a distance of at least two meters apart from each other. After connecting these to the build-up datalogger, a first run, called *parallel test,* is started (see Fig. 1.6).

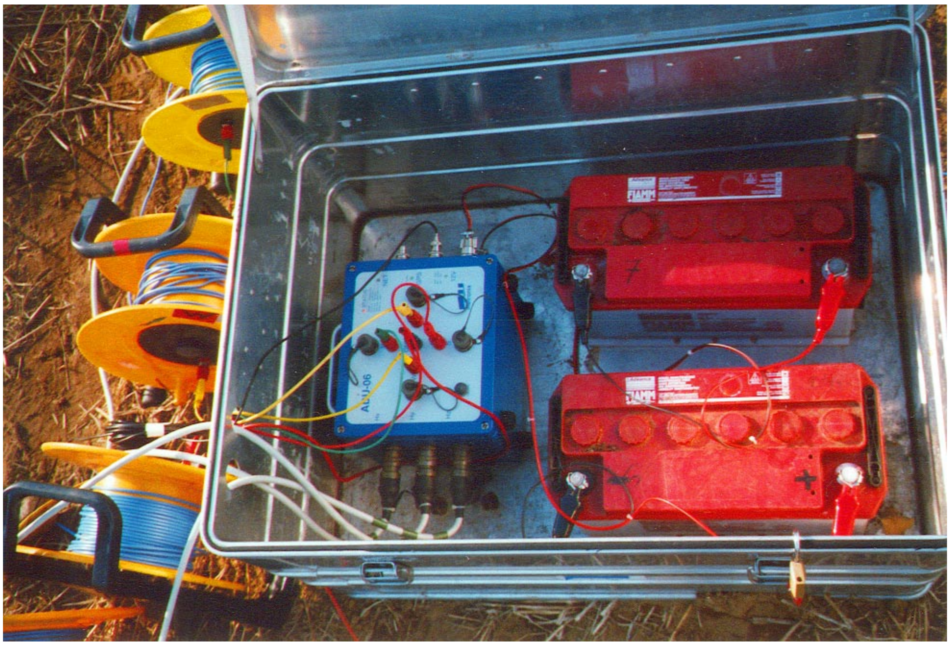

Figure 1.6: Datalogger in its aluminum box in field operation

Due to the parallel orientation all magnetic components have to show the same signal on the laptop display (see Fig. 1.7). Some noise may be caused by disturbances due to mechanical vibrations of the ground, particular caused by wind . The signal can now be checked for contact problems due to broken cabels or any corrosion of the contacts, and whether the chopper is working or not.

The signals have to be checked for any disturbances *(signal test),* such as

- anti-corrosion signals of gas pipelines
- electrical driven fences in fields
- disturbances from settled areas
- any other artificial signal.

When the signal is clear and there are only undisturbed oscillations, which can be identified as required source signal, the coils can be set up into their

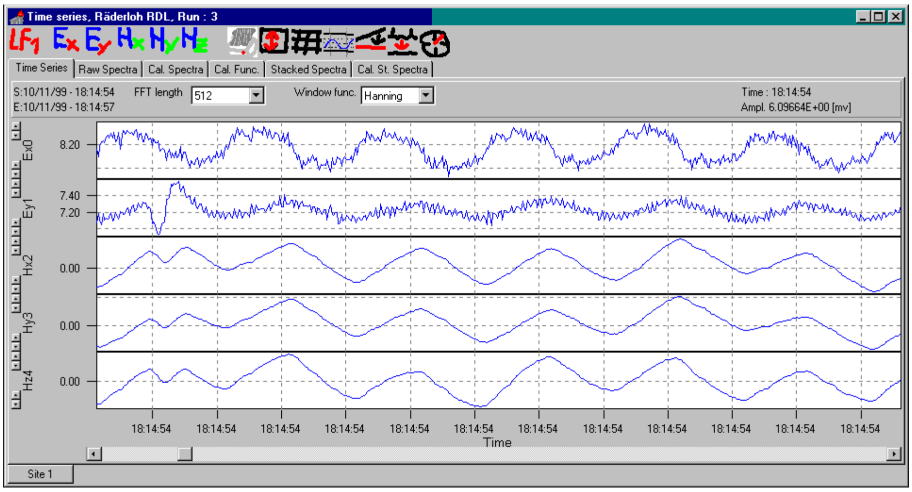

Figure 1.7: Segment of a time series during the *parallel test* of the magnetometer. The electrodes measure the signal already in their final position

final position. Therefore they must be placed as far away as possible from the datalogger to reduce the noise for any additional disturbing source. The coils have to be dug exactly towards north, east and vertical direction. This can be checked by a compass and level.

Figure 1.8 displays a segment of a time series measured by a 2 Hz sampling rate. The sensors picked up a strong signal with period of about 40 s, which

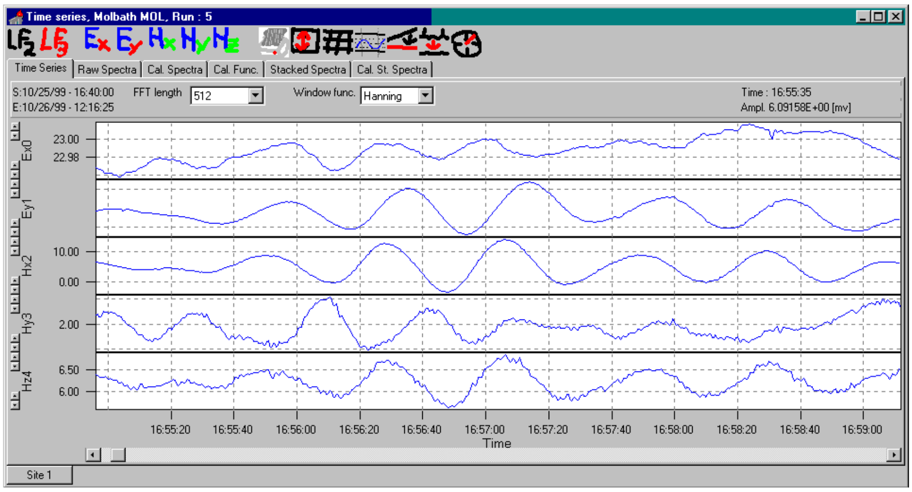

Figure 1.8: Clipping of a time series with E_x, E_y, H_x, H_y and H_z measured directly by the input channels in millivolts

might be interpreted as a continuous pulsation of type *pc3*. The amplitudes of the measured signals are displayed directly in millivolts. The correlations between the channels for E_y and H_x can clearly be recognized with a phase shift of about 45°. Channels for E_x and H_y seem to be weaker excited by the dominating source in this example. The presentation is automatically autoscaled, but here the noise is much stronger compared to the other signal. H_z is dominated by incoming signal of H_x due to the stronger excitation.

After measuring all band configurations a processing can be performed. Figure 1.9 shows the transfer functions in terms of apparent resistivity and phase for all bands fitted together of the station Gusborn (derived by MAPROS). The

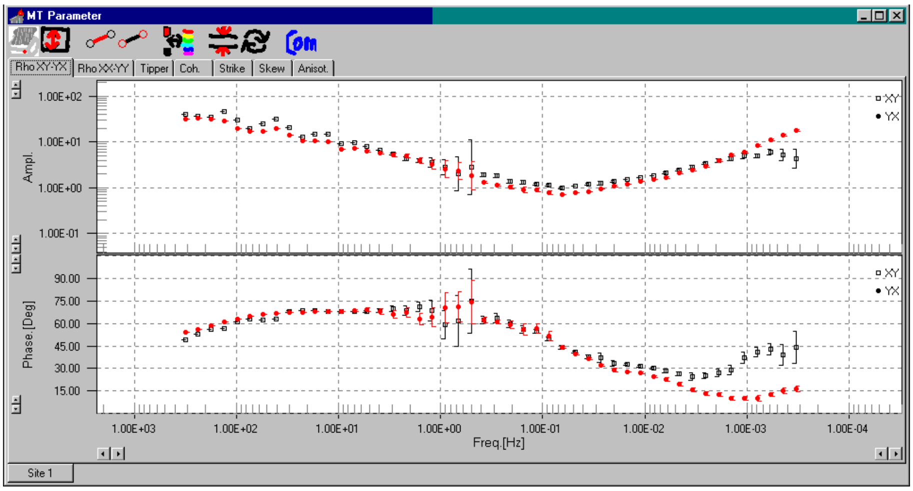

Figure 1.9: The transfer function of station Gusborn after being processed by the commercial software MAPROS of Metronix

software MAPROS also enables the user to perform a manual selction to events to be excluded from processing:

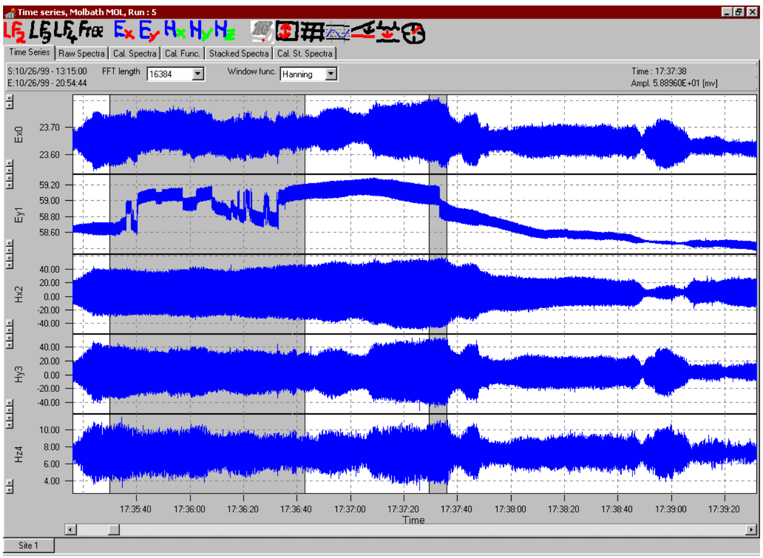

Figure 1.10: Manual selection

Chapter 2

The Survey

The German Federal Institute of Geosciences and Natural Resources (BGR) is working for years to complete the geological information of Nothern Germany by magnetotelluric measurements. Several surveys have been acquiring data of 88 magnetotelluric sites in the North German Basin from 1993 until 1995. An overview of these previous surveys, serving an integrated geological and geophysical modelling, has been reviewed in HOFFMANN et. al. (1998).

This survey has been carried out by **Metronix** from October 1999 until February 2000 and covers a region from Celle to the Lower Elbe Line. I have been in charge of planning, managing and setting up these sites in field. The data acquisition has been supervised by Dr. B. Friedrichs, **Metronix**.

This chapter gives a review and discussion of the acquired data. The interpretation at the end of this chapter is just a preliminary view and is based on the heuristic $\rho^* - z^*$-transformation and 1D inversions.

2.1 North German Basin

The terrain of interest is known as the North German Basin. The Basin has been covered by sea in its historical epoch. We have a top layer consisting of sand materials of previous ice ages and covering thick layers of sediments. The total thickness of the crust is assumed to be around 30 km.

The topping layer is of greater resistivity, while the sedimentary materials respond as a good conductor. The sedimentation process leads to layered formation. The lower formation is reported to show anisotropic effects combined with an increasing resistivity. The basin is supposed to show a strike direction from southeast to the northwest for high frequencies.

Since 1993 measurements of magnetotelluric sites in Northern Germany provided data on several lines (see Fig. 2.1). An example of a segment of a resulting combined geological and magnetotelluric model due to a previous evaluated survey is shown in Figure 2.2 (HOFFMANN et al. 1998). This data acquisition is intended to complete a section between previous measured lines.

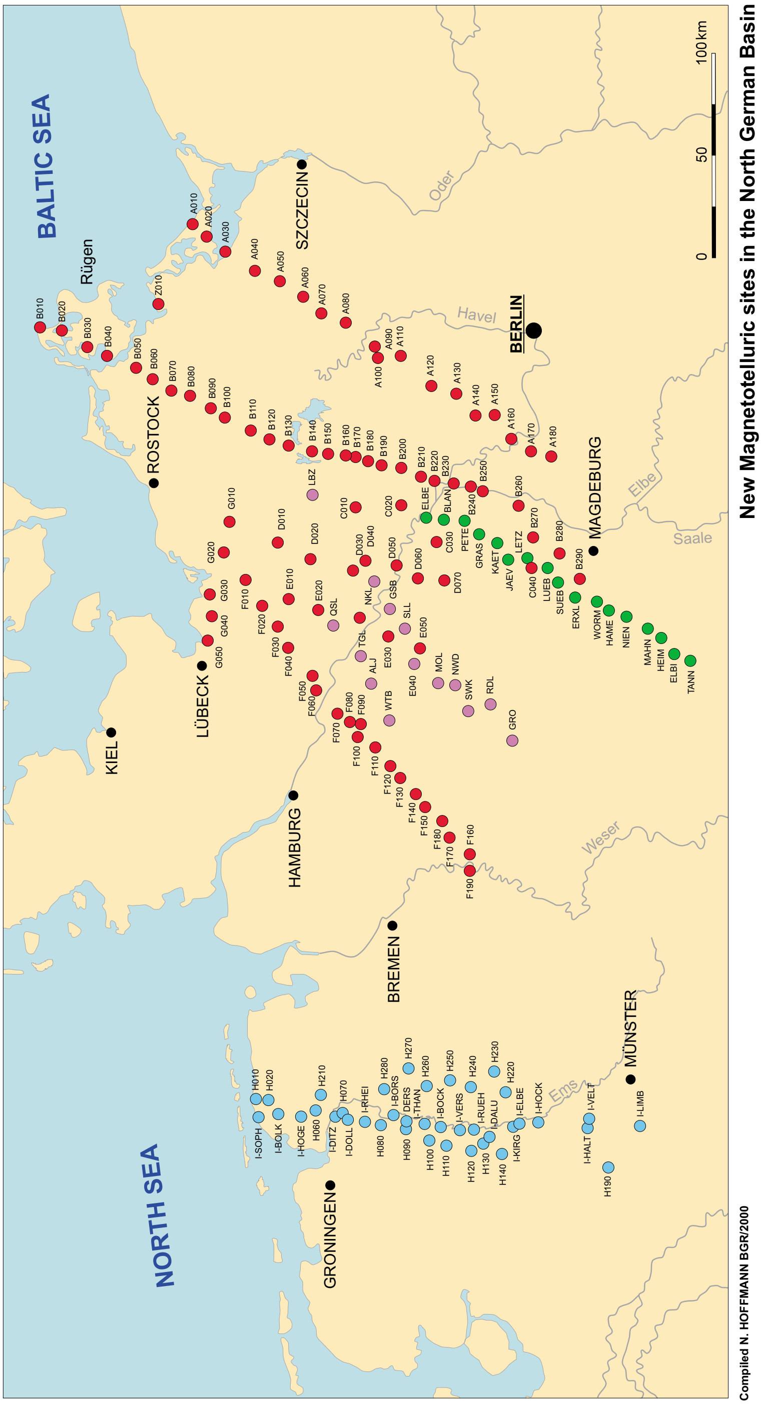

Figure 2.1: All measured magnetotelluric sites in Nothern Germany since 1993. The sites of this actual survey painted in purple (Courtesy of Hoffmann, BGR (not yet published)

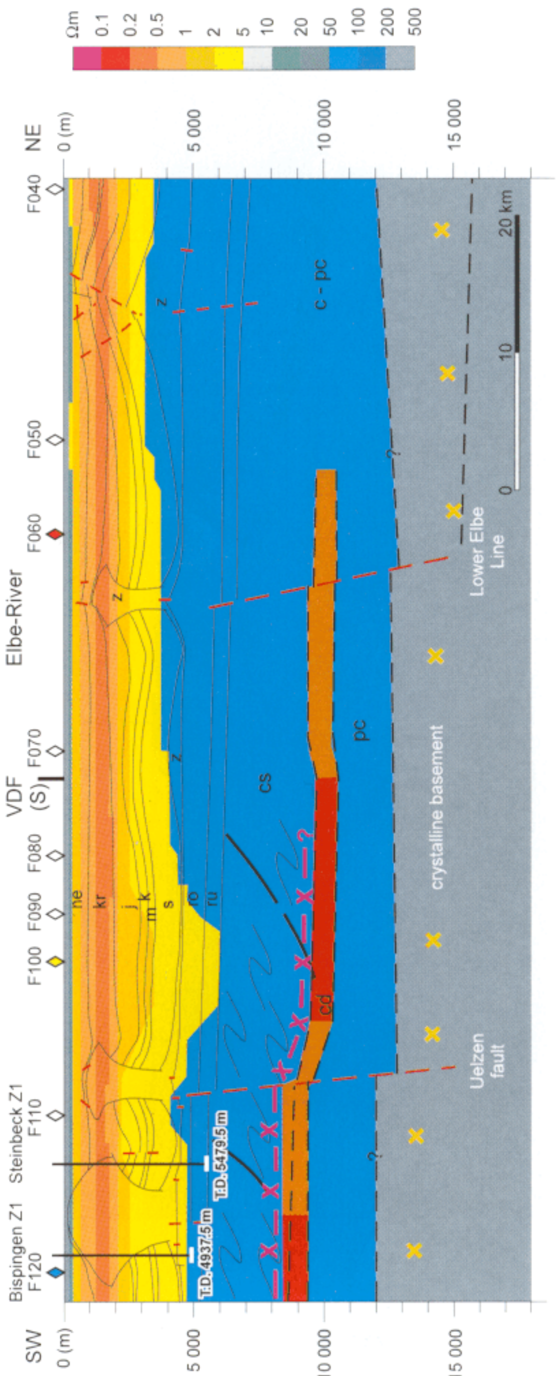

Figure 2.2: A segment of a combined geological and magnetotelluric model of a previous measured line ranging from Wismar to Nienburg. (Courtesy of Hoffmann, BGR)

2.2 Data acquisition

The survey includes 14 stations spread over two parallel lines enumerated Line 1 and Line 2 (see Fig. 2.3). The average distance between these sites is around 10 km. Local artificial leads to deviations from the line.

Line 1, containing 10 stations, started south of Wathlingen, Celle and ended at Neu Kaliß, northeastern of the Elbe river. Strong disturbances eastward of the Elbe river led to the decision to start a second line and skip the planned stations between Neu Kaliß and the last station already measured at Lübz. The second line contained 4 stations from Wettenbostel to Quassel, east of the Elbe river. The stations are summarized in Table 2.1.

	Station	Abbr.	Duration (date)	rm-rf with	Remark for rm-rf
Line 1					
1	Wathlingen	WTL	07.10 - 11.10	2	disturbed
2	Groß Oesingen	GRO	21.01 - 26.01	9	ok
3	Räderloh	RDL	15.10 - 19.10	-	remote error
4	Schweimke	SWK	21.10 - 24.10	8,5	ok
5	Nienwohlde	NWD	24.10 - 28.10	5,6,8	ok
6	Molbath	MOL	25.10 - 30.10	5,7	ok
7	Sallahn	SLL	28.10 - 31.10	6	ok
8	Gusborn	GSB	21.10 - 26.10	4,5	ok
9	Neu Kaliß	NKL	21.01 - 26.01	10,2	ok
13	Lübz	LBZ	31.10 - 04.11	9	disturbed
Line 2					
14	Wettenbostel	WTB	17.02 - 21.02	16	ok
15	Aljarn	ALJ	03.02 - 08.02	-	remote error
16	Tosterglope	TGL	17.02 - 21.02	14,17	ok
17	Quassel	QSL	17.02 - 21.02	16	ok

Table 2.1: Stations measured. Duration time considers the selected long term runs LF 3 used for processing.

A standard measuring program has been executed to cover a spectrum beginning at a few hundred Hz down to about 4000 s (see Tab. 2.2). About

Band	F_s [Hz]	T	Type	Data amount
LF 1	4096	10 min	single	$\sim$ 25MB
F 512	512	10 min	single	$\sim$ 25MB
LF 2	64	8-12 h	single	$\sim$ 10MB
LF 3	2	3-5 d	remote	$\sim$ 0.5kB

Table 2.2: Configuration of measuring tasks. LF 4 has been generated by filtering of LF 3.

2 Gigabyte of data has been acquired during this survey.

Parallel measurements for remote reference has been realized considering the long term runs (LF 3). Several failures of stations caused a lack of remote

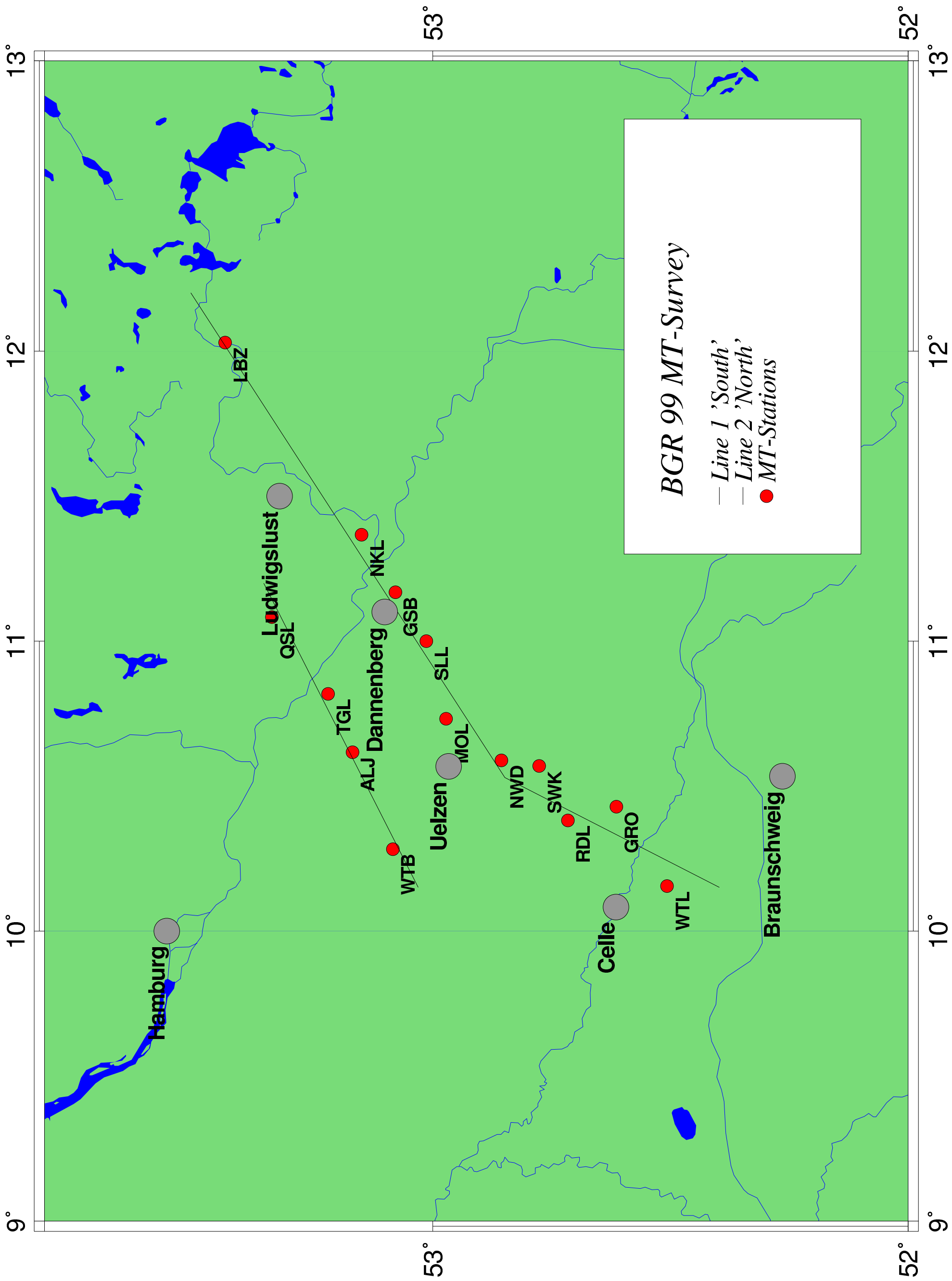

Figure 2.3: The magnetotelluric sites spread over two lines of this survey

partners for station 3, Räderloh (RDL) and station 15, Aljahrn (ALJ). The single-site method led still to acceptable response functions. Wathlingen has been disturbed by temporary contact problems, which demanded manual selection of the time series segments. This is possible with software like MAPROS, but not with automatic processing codes. This interpretation covers only data being processed by the code of Jim Larsen. Therefore station Wathlingen and Lübz have been dropped here.

Now we take a closer look on the magnetic excitation as provided by the Kp indices[1] as a measure for the planetary activity. The Kp indices for september to December 1999 have been downloaded from the server of the Institute of Geophysics in Göttingen and are displayed in Figure 2.4. A lack of excitation can

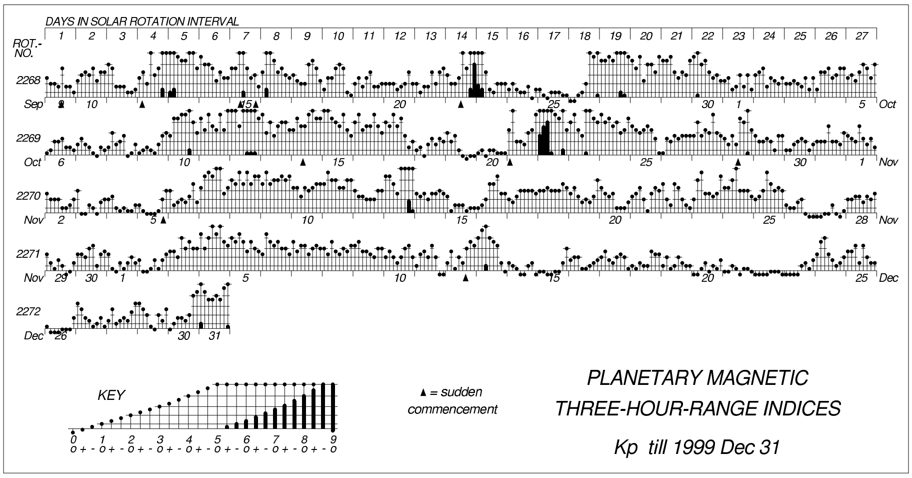

Figure 2.4: Kp-Indices of september to December 1999

be recognized during 18th until 20th of October and 2nd until 5th of November. This correlates with the data quality of stations which have been measuring at these days (e.g. station 13). The remaining time of October 1999 and the later measurements in January and February 2000 have been excited well.

2.3 Data Processing

The data processing has been executed with the processing code provided by Jim Larsen. The handling of this code is described in Appendix **??**. The data output is provided by the processing as magnetotelluric impedance Z_{ij} [km/s] for all tensor components as well as the tipper T. In Appendix Athe response

1

Kp indices: The global activity of excitation can be judged by the geomagnetic planetary indices (Kp). The planetary three-hour-range Kp indices have been introduced by J. Bartels in 1949 and is derived from the standardized K indices (Ks) of 13 magnetic observatories. It is designed to measure solar particle radiation by its magnetic effects. (Taken from the data description of the server) functions are summarized in terms of apparent resistivity and $\rho^* - z^*$.

The processing code needs to be executed with predefined parameters. In general these have been chosen for a FFT window length of 1024 data points and a desired decimation factor of 2. A first difference for reducing pipline noise has not been processed. The rotation has been fixed to north (respectively east) whereas the code allows a rotation to the maximum and minimum directions of noise. Only the 50 Hz line has been removed. The removal of the net current of the railway system (16 2/3 Hz) did not improve the processing results. The data had to be orthogonalized, as the code output is orientated for the electric direction related to the magnetic axis of major and minor of coherency (see Appendix ??).

The short term runs have been measured individually without a remote partner. The long term runs (2 Hz and below) have been processed by the remote reference technique - except for two stations. The data quality of the processing results of station Wathlingen (WTL) and Lübz (LBZ) have been too bad, so they were not taken in further consideration. This has been caused by local multiple coherent noise in Lübz and temporary contact problems of the electric sensors in Wathlingen.

A few remarks have to be added considering the general data quality of apparent resistivity of the remaining stations. The dead band effect caused a general uncertainty of the data in the spectra of a few Hz to 10 s. The data for the highest frequencies do not seem to be plausible for all stations. We omit these and only consider data below 300 Hz as reliable.

2.4 Data Interpretation

Looking on the unrotated apparent resistivities two things can be emphasized immediately. First, it can be realized that the data have an almost similar shape. This indicates that all stations roughly describe an almost similar structure of the subsurface. Second, both polarizations, Z_{xy} and Z_{yx}, are congruent for frequencies above 10 s and split for the lower frequencies. This behavior roughly suggests that a 2D structure in the deeper ground is being covered by a 1D layered structure.

2.4.1 $\rho^* - z^*$-interpretation

The data is displayed in unrotated $\rho^* - z^*$-presentation in a line configuration for both profiles in Figures 2.5 and 2.6.

Already at a first glance a tripartite sequence consisting of a poor-good-poor conductor can be identified. This applies to the example of a three-layer-model as introduced for the $\rho^* - z^*$-interpretation. Second, an lateral inhomogeneity effect can be recognized, increasing from southwest to northeast. Third, the last four stations (s06-s09) of the southern line seem to be consistent in their $\rho^* - z^*$-relation with the stations (s14-s17) of the northern line. This indicates that both lines cross the same structure in a parallel sections at different places.

Back to the well conducting layer, it can be realized that this one is thicker in the north-eastern region than in the south-western and finally seems to vanish at

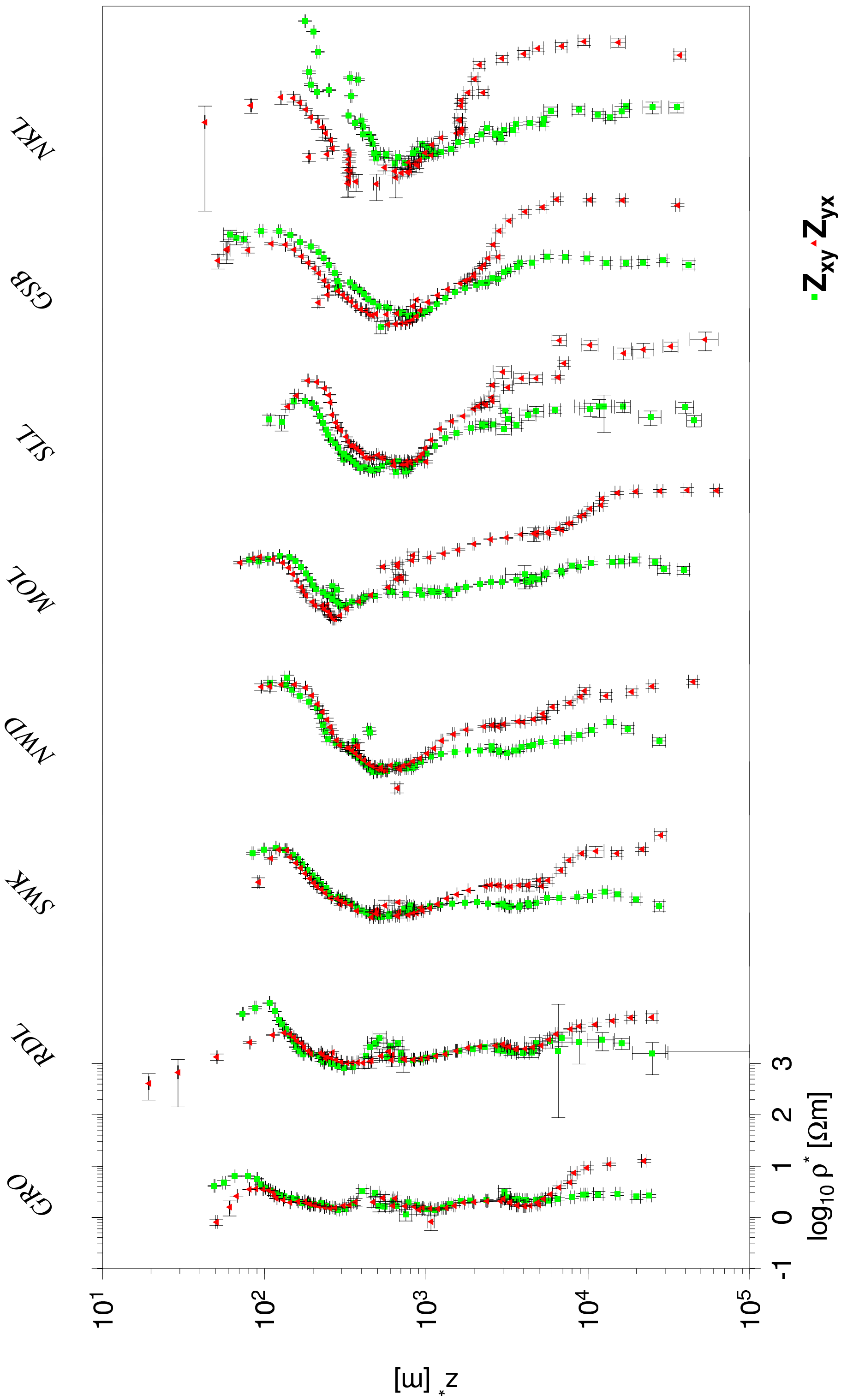

Figure 2.5: $\rho^* - z^*$ presentation of Line 1 'South'

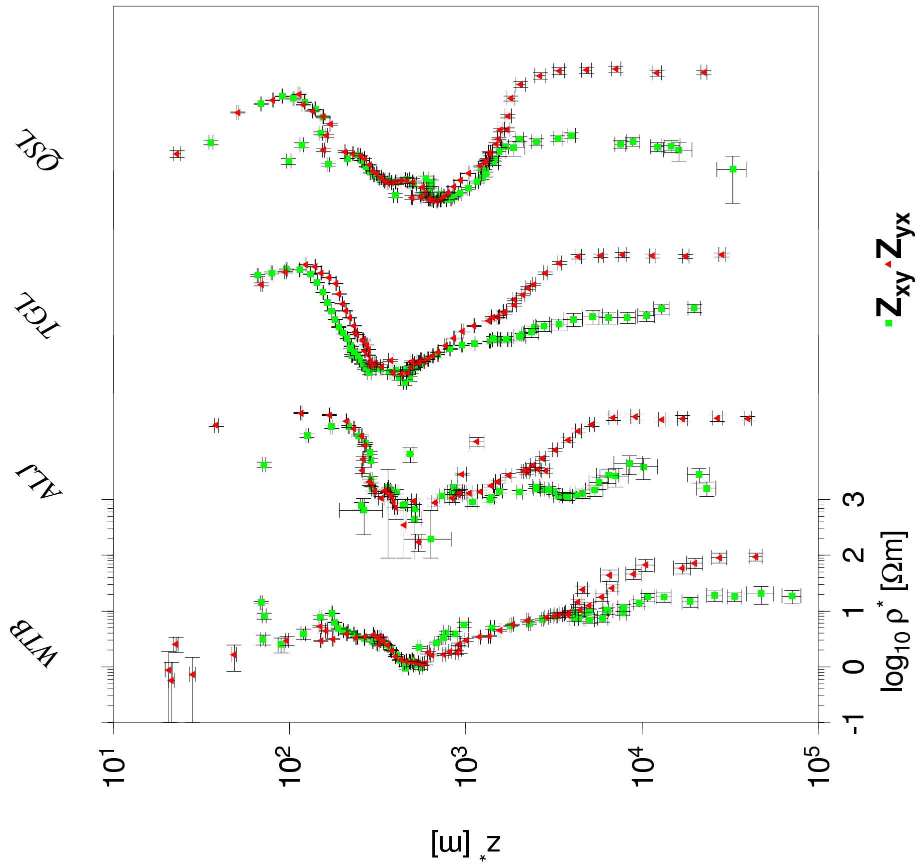

Figure 2.6: $\rho^* - z^*$ presentation of Line 2 'North'

station Groß Oesingen (GRO). The remaining data of Z_{yx} of station Wathlingen (WTL) seem to confirm this tendency. The thickness of this layer seems to decrease for the two parallel stations Molbath (MOL) at Line 1 and Wettenbostel (WTB) at Line 2.

The collection of all observations gives a basic idea of a conductivity model of Line 1 sketched in Figure 2.7. Line 2 corroborates this model.

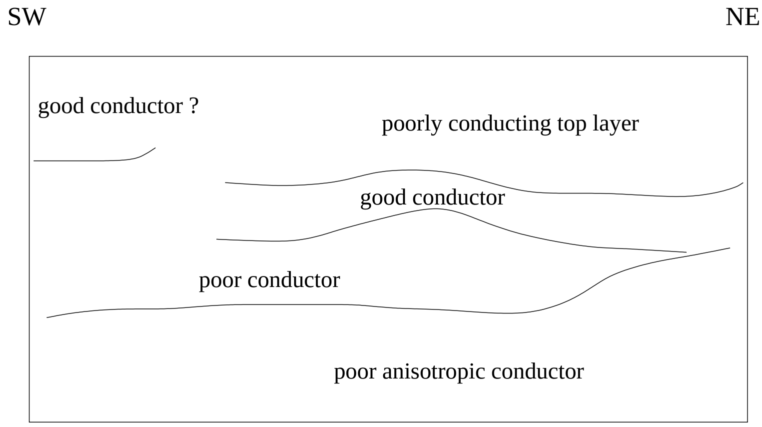

Figure 2.7: A first heuristic sketch of a conductivity model assumed by the $\rho^* - z^*$-interpretation

2.4.2 Induction arrows

The induction arrows have been processed by the robust code of Jim Larsen. These have been band averaged for different presentations. In Figures **??** to **??** band averaged induction arrows are displayed for every half decade of each single station. Figures A.6 to A.8 present decade-averaged induction arrows for each band on a map of the survey area.

Five bands have been defined to simplify the presentation. Band 1 collects frequencies from 300 Hz down to 10 Hz. Bands 2 to 4 average a whole decade, while the last band collects all frequencies below periods of 100 s. To estimate the inductionspace Table 2.3 lists the range of derived z^* from measured data. Bands 1 and 2 consists of high frequencies and therefore represent only local

Band	$f_{\max}$	$f_{\min}$	$z^*_{\max}$	$\delta_{\max}$
1	300 Hz	10 Hz	~100-300m	~200-600m
2	10 Hz	1 Hz	~200-500m	~400-1000m
3	1 Hz	10 s	~ 800-1 km	~ 1.5-2 km
4	10 s	100 s	~ 2-3 km	~ 4-6 km
5	100 s	4000 s	~ 20-30 km	~ 40-60 km

Table 2.3: Penetration and skin depth for the single bands

information. The low-frequency data as in Band 4 and 5 contain the regional information.

At first we focus on the induction arrows for each single station. Three stations - NKL (s09), ALJ (s15) and QSL (s17) - present very huge induction arrows for high frequencies. They remain huge in the full frequency range only for QSL remains unexplained. Since high frequencies just represent local information, the effect in Neu Kaliß (NKL) and Aljarn (AlJ) is no of interest. Following stations show slow and consistent movements of the induction arrows in spectral progression: NWD (s05), SLL (s07), GSB (s08), TGL (s16) and even QSL (s17). Figure 2.8 for station Sallahn (SLL) presents the slow turn of the induction arrows from northwest for the higher frequencies to the southeast for the lower.

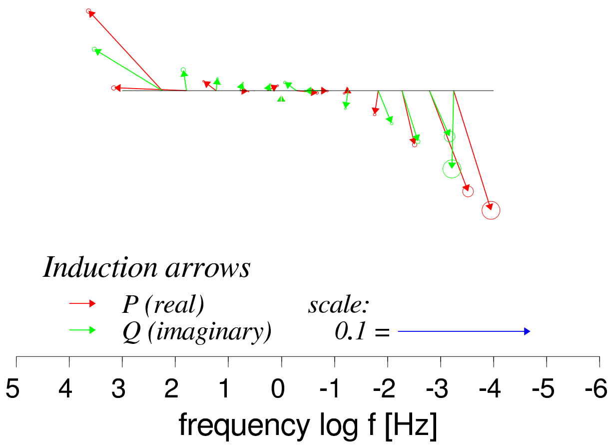

Figure 2.8: Induction arrows of station Sallahn

Most high frequent induction arrows, as averaged in Band 1, point in a northwestern direction. This could be explained by a continuous surface conductivity gradient from southeast to northwest

The induction arrows of Bands 2 to 3 are smaller than 1 and 5, suggests a 1D-like layered structure for a frequency range from 100 Hz to 100 s. Station Sallahn demonstrates this quite well (see Fig. 2.8). This can be explained by the underlying sedimentary layers.

The induction arrows for the lowest frequencies show a typical behavior. According to Figure 2.9 the induction arrows of most stations turn south. This has been reported in many studies.

The penetration depth reaches the ground of the basin and is influenced by its underlying structure.

2.4.3 1D Interpretation

Looking at the apparent resistivities of the stations, the polarizations split only for periods higher than 100 to 10 s, depending on the individual station. But the data seem to be congruent for smaller periods.

For reasons of stability, the determinant of the impedance tensor, according to Berdichevsky & Dmitriev (1976) as given in equation (**??**), for frequencies from 300 Hz to 100 s has been computed. This invariant averages the data and provides an rotationally invariant response function.

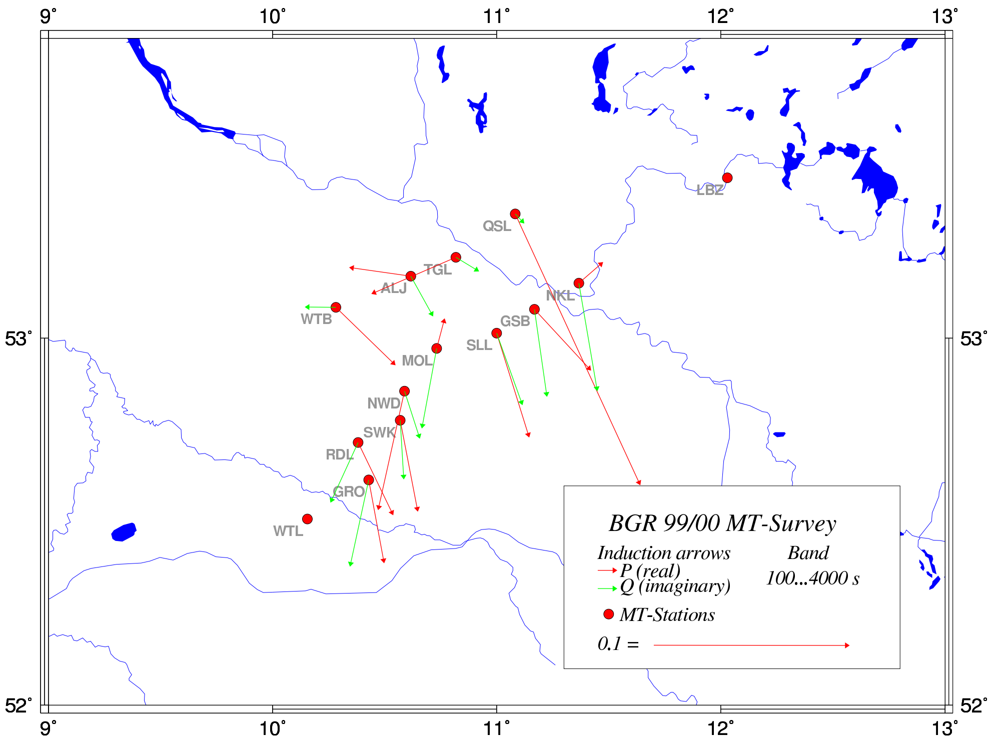

Figure 2.9: Induction arrows of Band 5 for periods 100 s to 4000 s pointing southward for most stations

Based on these data D^+-models have been computed and plotted in terms of cumulative conductance in Figure 2.10. The individual 1D models for each station of Line 1 and Line 2 are displayed in Appendix A in Figures A.9 and A.10. A starting vertical line indicates a well-conducting layer at the surface, while a terminating horizontal line in the depth indicates a final perfect conductor at the bottom.

Looking at the summarized 1D models in Figure 2.10 we recognize a common increase of conductance up to values of several thousands Siemens for the selected data. Most stations show a rapid increase of conductance in the upper region, but the rate declines.

The conductivity is derived by

$$\sigma(z) = \frac{d}{dz} S(z).$$

The graph displays the depth z, pointing downward, versus the cumulative conductance as a staircase function.The conductivity is determined by the slope of a regression line for a selected number of steps. The selection of the steps is to a certain extent arbitrary and leads to a non-unique interpretation. This is in accord with a result of Berdichevsky & Dmitriev (1992) that the inverse problem for the cumulative conductance $S(z)$ is well posed, whereas the inverse for $\sigma(z) = S^{'}(z)$ is ill-posed.

Due to this presentation a steep slope represents a low conductivity, while a gentle slope represents a higher conductivity.

These regression models provide mostly a poorly conducting layer covered by a well conducting layer. It is very difficult to average a slope based on the deepest steps. Some might suggest a underlying good conductor as a bottom layer.

2.4.4 Assumed Electrical and Magnetical Properties

Material	Dielectric constant ϵ_r
Granite(dry)	4.8-18.9
Gabbro	8.5-40
Basalt	12
Sandstone	4.7-12
Gneiss	8.5
Peridotite	8.6
Water(20°C)	80.36
Soil	3.9-29.4
Clays	7-43
Quartz	4.2-5

Table 2.4: Some dielectric constants taken from lecture notes of H.Brasse (referring to Telford et al. 1992)

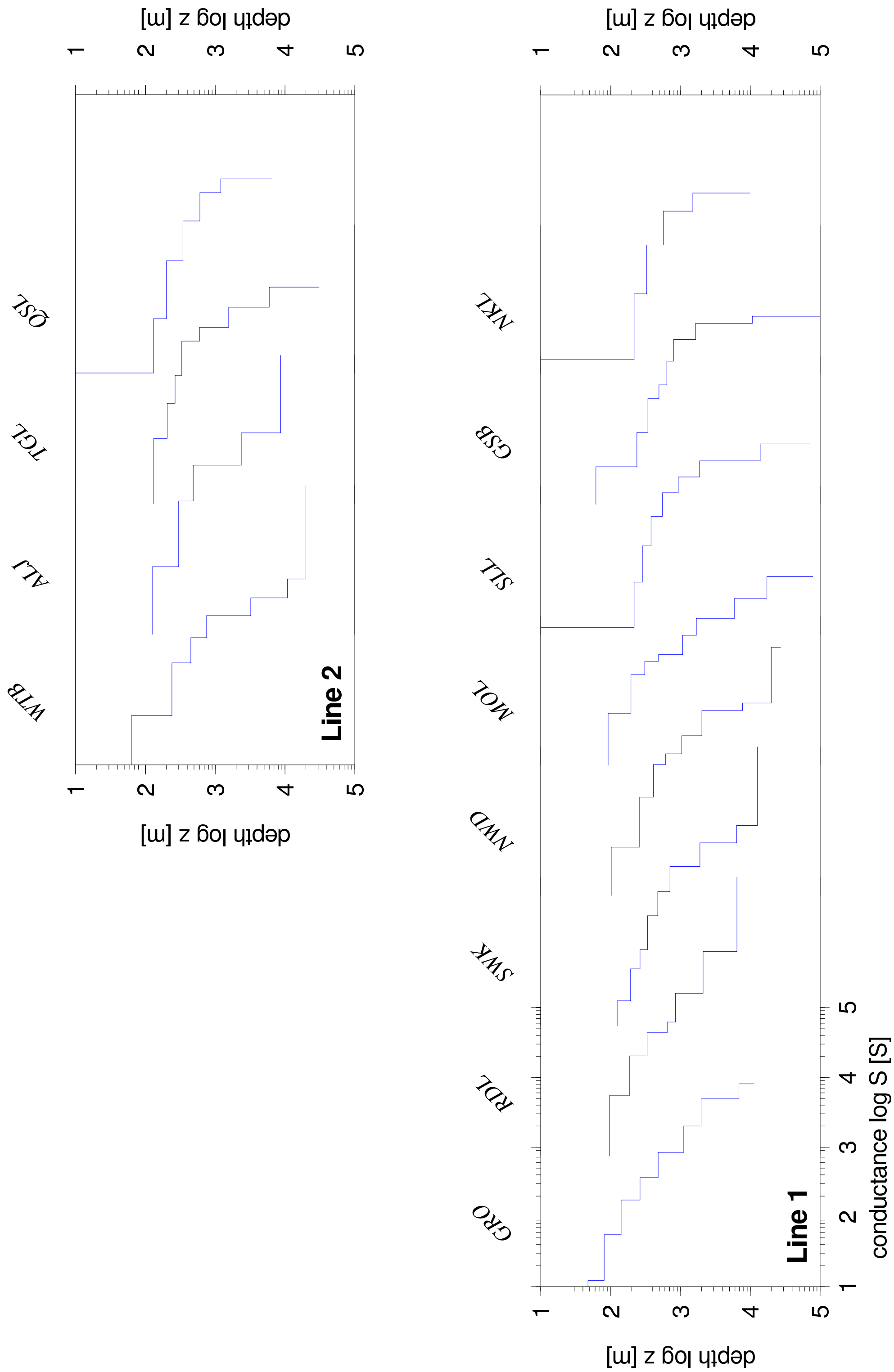

Figure 2.10: 1D models in presentation of cumulative conductance

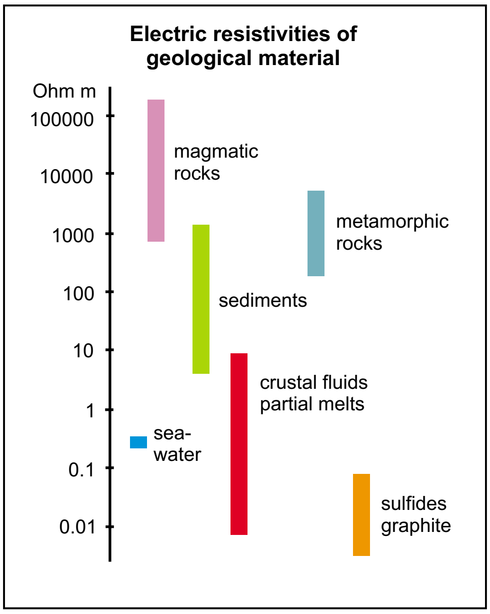

Figure 2.11: Ranges of electric resistivity (the reciprocal of conductivity) of geological media (Lecture notes of H. Brasse)

Material	Magnetic permeability μ_r
Magnetite	5
Pyrrhotite	2.55
Titanomagnetite	1.55
Hematite	1.05
Pyrite	1.0015
Rutile	1.0000035
Calcite	0.999987
Quartz	0.99985
Hornblende	1.00015

Table 2.5: Some magnetic permeability taken from lecture notes of H.Brasse (referring to Telford et al. 1992)

2.4.5 Sources and spectra of excitation

Sources of excitation can be located either internally or externally. Internal sources are caused by secular variations of the geomagnetic fields. Their spectral activity cover periods beneath four years and are therefore of minor interest. External sources are caused by inducing currents in the ionosphere and/or magnetosphere, tidal induced (Junge 1993) and atmospheric electricity. Figure 2.12 shows a segment of the spectral activity. The magnetic and the responding

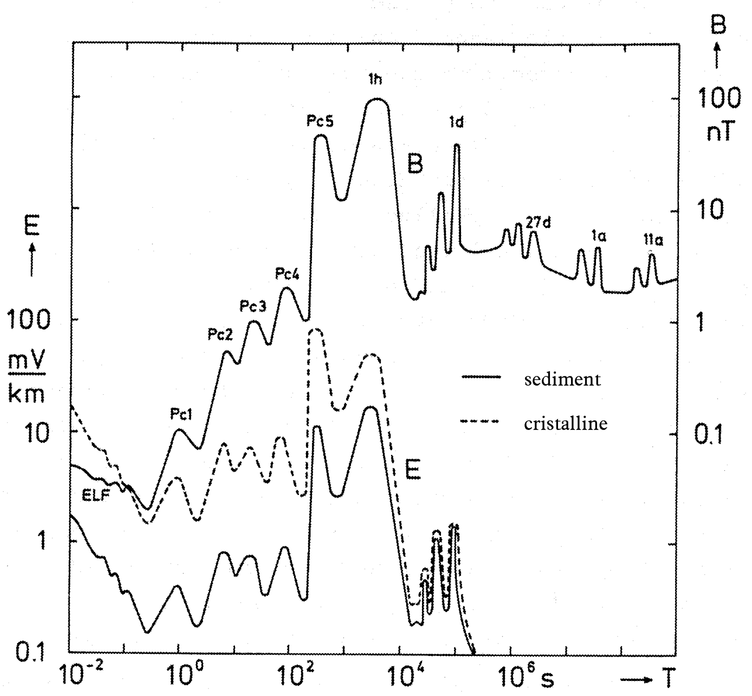

Figure 2.12: Spectra of magnetic field and the responding electric field in ground (Lecture notes of WEIDELT)

electric field for two different media are overlayed in this plot. The magnetic field consists of the exciting part and its magnetic response due to the induction process. The spectral transfer between the magnetic field and the electric response can clearly be recognized.

An almost complete list of natural variations of interest is summarized in Table 2.7 and 2.8 including their spectral activity, amplitude and source location. Due to the interaction between the solar wind and the magnetic field of the earth, currents are caused in the magnetosphere and ionosphere. These currents provide the exciting magnetic field on the ground. Complicated external fields above the ionosphere can be presented by equivalent sheet-currents in the ionosphere due to the potential theory.

At last, effects caused by artificial sources like power lines (net current) have to be considered for further time series processing. There is a lack of excitation in the period ranges of 1 s to 10 s between pc 1 and pc 2 which is called *dead*

1. Irregular variations	Abbr.	Period/Freq.	B [nT]	Source location
high frequent emission and whistler spherics	VLF	10 μs-1 ms 3 kHz	$\ll$0.1	magnetosphere, lighting
low frequent emissions and atmospherics	ELF ULF	3 kHz-1 Hz >1 s	<0.1	atmosphere, lighting
SCHUMANN resonance		5/39 s ...	<0.1	wave guide earth-ionosphere
continuous pulsations irregular pulsations	pc1-5 pi1-2	0.2-600 s 1-150 s		magnetosphere -"-
solar flare effects	sfe	10 min	10	ionosphere, D&E layer
sudden storm commencement	ssc	2-5 min	10-100	magnetosphere
polar sub storm without recovery phase polar electrojet	bay PEJ	30-120 min 30-120 min	20-100 20-100	ionosphere of the auroral zone magnetosphere
polar magnetic storm with recovery phase	DP (PEJ)	5-120 min 5-120 min	20-100 20-100	-"- -"-
recovery phase of polar magnetic storms	Dst DS	3 d 1 d	100 100	ring current ring current
equatorial electrojet	EEJ	all freqs.		ionosphere at equator
2. Regular variations	**Abbr.**	**Period/Freq.**	**B [nT]**	**Source location**
solar daily variation - on quiet days	S Sq	1 d 1 d	20 20	E-layer in ionosphere -"-
lunar daily variation	L	1 d	2	E-layer in ionosphere
semiannual variation		6 months	5	ring current
annual variation		1 a	5	ionosphere
sunspot cycle variation		11 a	20	ring current

Table 2.7: External sources of natural excitation (Schmucker, lecture notes winter term 92/93)

	pc-1	pc-2	pc-3	pc-4	pc-5	pi-1	pi-2
T [s]	0.2-5	5-10	10-45	45-150	150-600	1-40	40-150
f [Hz]	5-0.2	0.2-0.1	100m-22m	22m-7m	7m-2m	1-0.025m	25m-2m
B [nT]	0.1	0.5		2	10	1	

Table 2.8: Ranges of periods and frequencies of different pulsation types

band.

Chapter 3

Conclusions

Due to the thesis I had the chance to participate in a survey applying the magnetotelluric sounding method for the German Federal Institute of Geosciences and Natural Resources (BGR). This survey has been carried out by **Metronix**, Braunschweig, with the latest equipment GMS 06. I have been in charge of planning, managing and setting up these sites in field, which have been supervised by Dr. B. Friedrichs, **Metronix**.

The survey covered a region in the North german basin southwest of the Lower Elbe Line including 14 sites spread over two lines. A basic $\rho^* - z^*$-presentation of the data suggests a regional tripartite sequence of a poor-good-poor conductor from the upper layer to the depth. The upper two conductors can be explained by layered media, whereas the underlying lower poor conductor shows the characteristics of a lateral inhomogeneity of the underlying basin.

D^+-models have been computed based on the congruent parts of the data from 300 Hz to 100 s. These models are presented in terms of cumulative conductance and show only the lower two layers as a good-poor conductor sequence. The interpretation of conductance model for a conductivity model remains ill-posed.

An algorithm for an error weighted decomposition of the magnetotelluric response function on the response of decaying eigenmodes for layered media has been implemented. Applying on measured data we obtain well-fitted curves excluding systematical errors, which are accompanied with greater statistical errors.

The adaption of the algorithm for an optimized spectral decomposition considering the presentation of the magnetic field for the TE-mode failed due to the fitting technique. It turned out that an alternative expression has to be fitted, which leads to a complicated non-linear problem.

For an outlook two subjects are to be pointed out:

- The acquired data are still subject for a future two-dimensional interpretation particularly concerning the lower-frequency data, which are related with the formation of the basin in depth. This interpretation will serve the completion of the combined geological and geophysical modellings for the North German Basin.

- The fitting algorithm for the MT impedance of excited free-decay modes for two-dimensional structures remains to be optimized. This could be achieved a by fitting technique with an enhanced fitting criteria as a subject of a non-linear problem.

Appendix A

Data Pool

A.1 Measured Data

The data, processed as magnetotelluric impedance, are presented as apparent resistivity and phase and their $\rho^* - z^*$-transform in Figures A.1, A.2, A.3, A.4, and A.5.

A.2 Induction arrows

For a geographical presentation the induction arrows have been averaged for five bands and projected on a map of the survey area in Figures A.6, A.7 and A.8.

A.3 D^+-Models

The D^+-models, as computed from the measured data of the frequency range from 300 Hz to 100 s, are displayed in Figures A.9 and A.10.

A.3.1 Phase and Resisitivity Sections

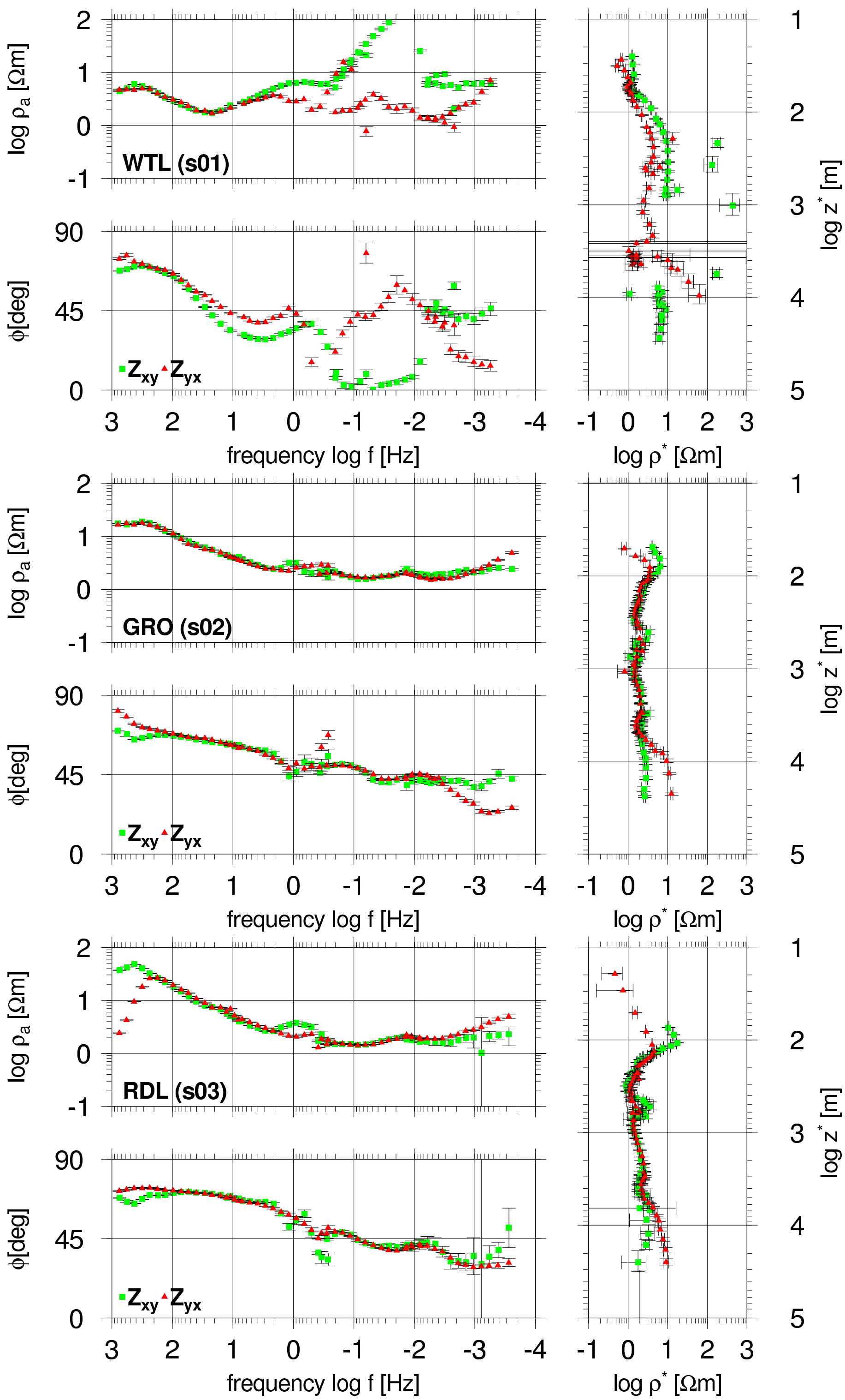

Figure A.1: Line 1, stations 1-3, not rotated.

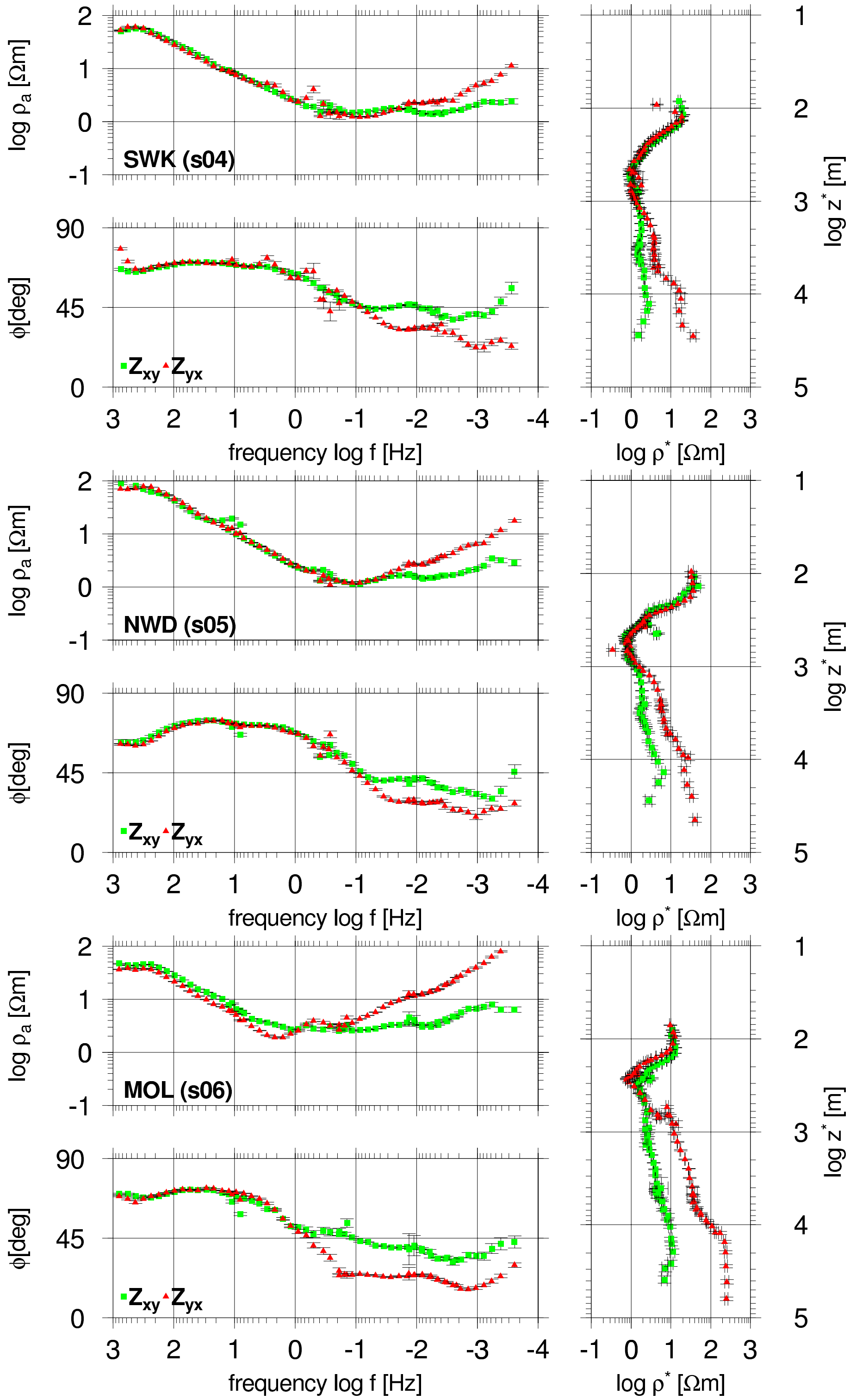

Figure A.2: Line 1, stations 4-6, not rotated

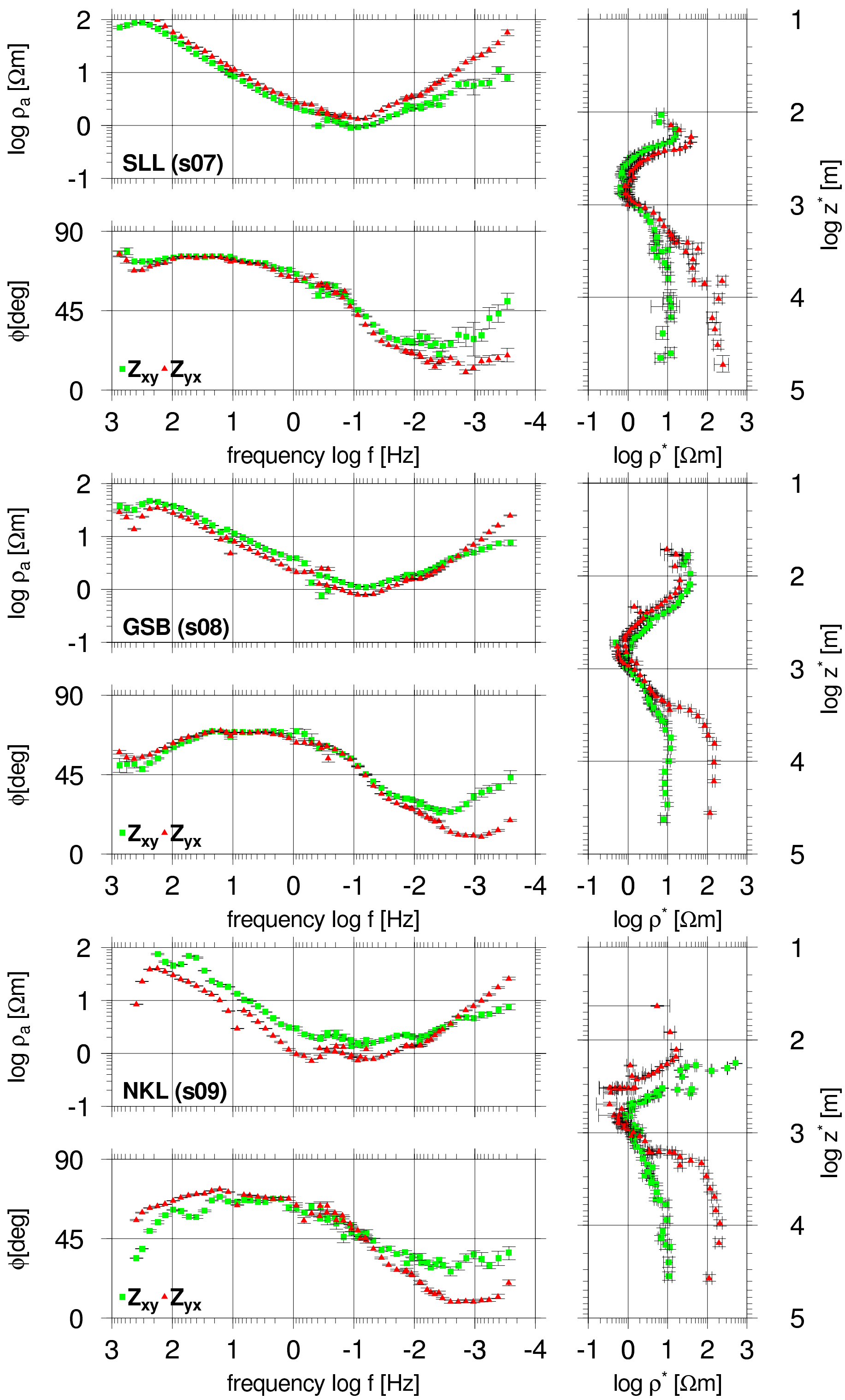

Figure A.3: Line 1, stations 7-9, not rotated

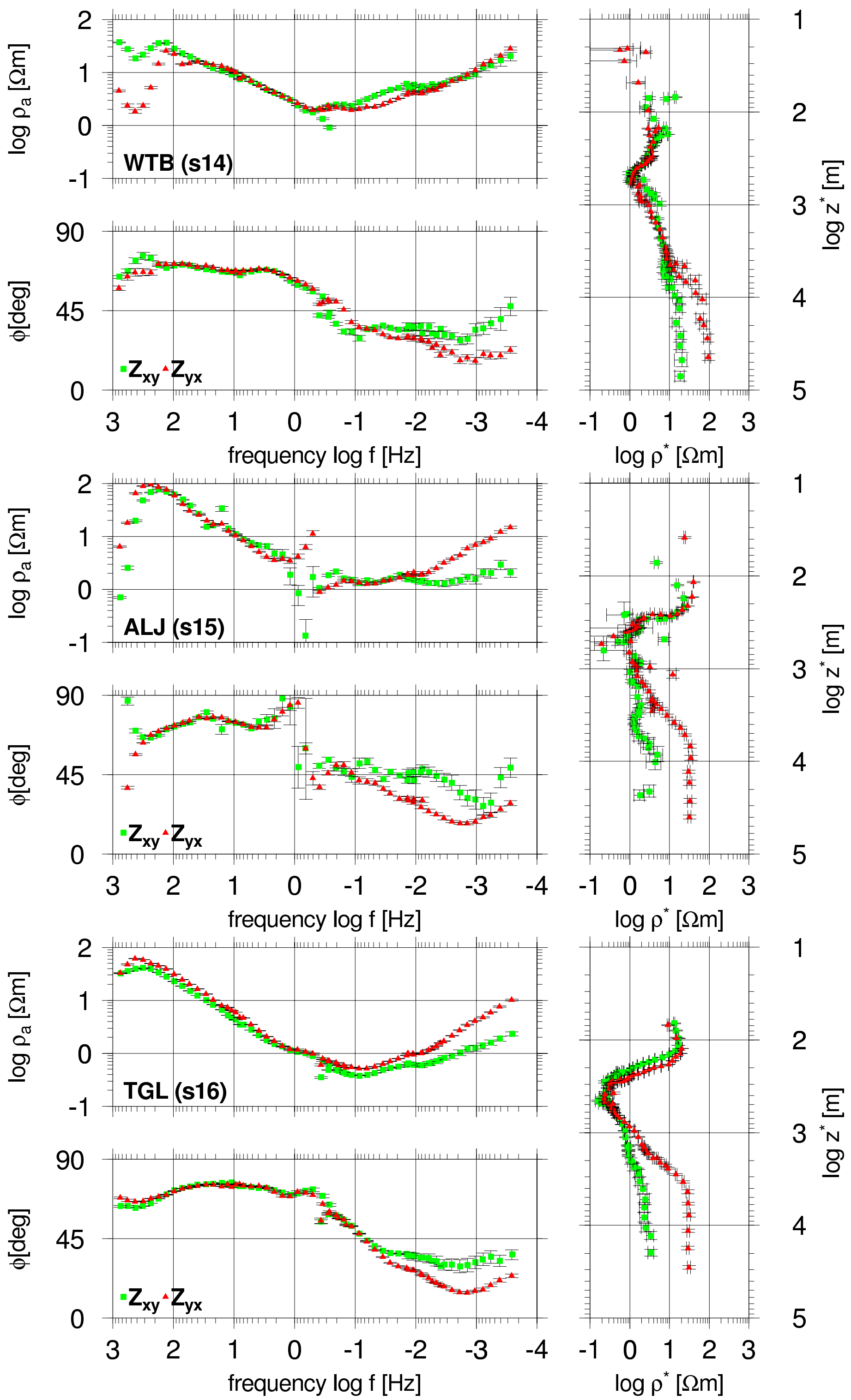

Figure A.4: Line 2, stations 14-16, not rotated

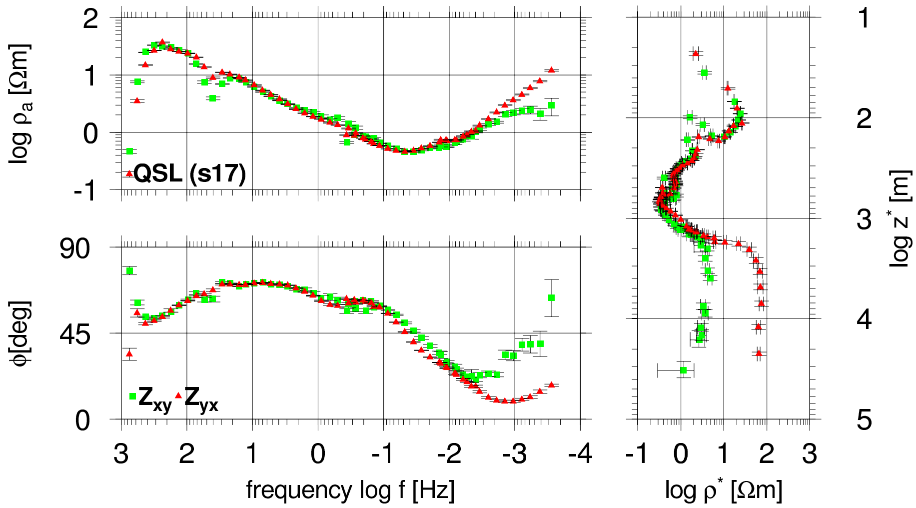

Figure A.5: line 2, station 17, not rotated

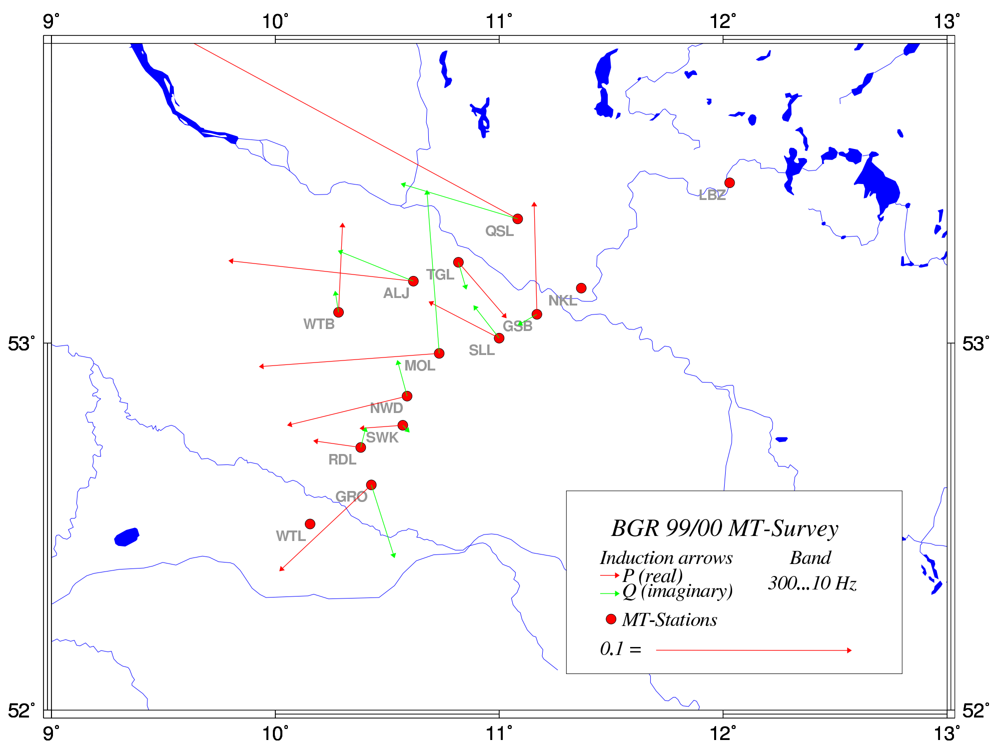

Figure A.6: Induction arrows, band averaged from 300 to 10 Hz

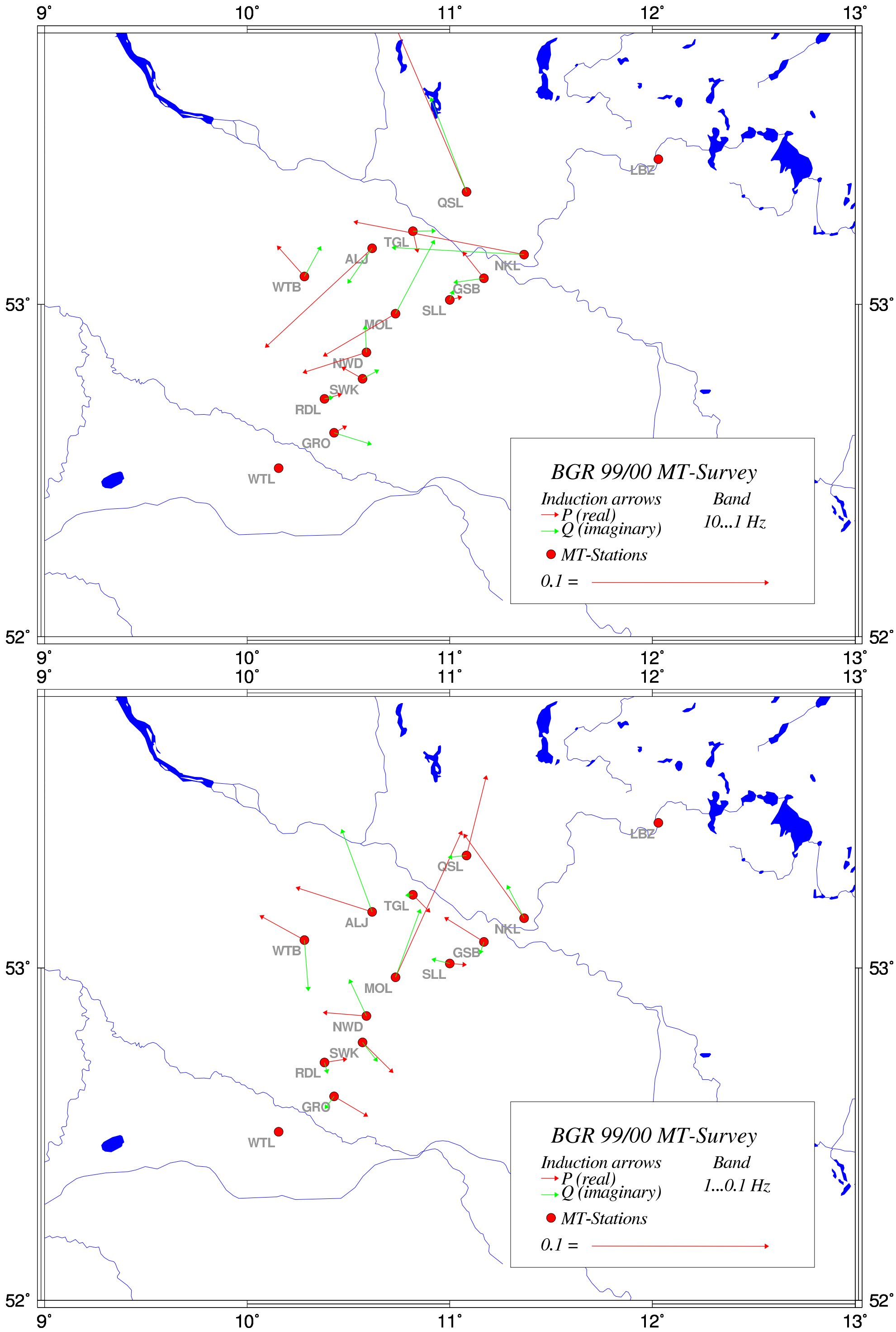

Figure A.7: Induction arrows, band averaged from 10 to 1 Hz and 1 Hz to 10 s.

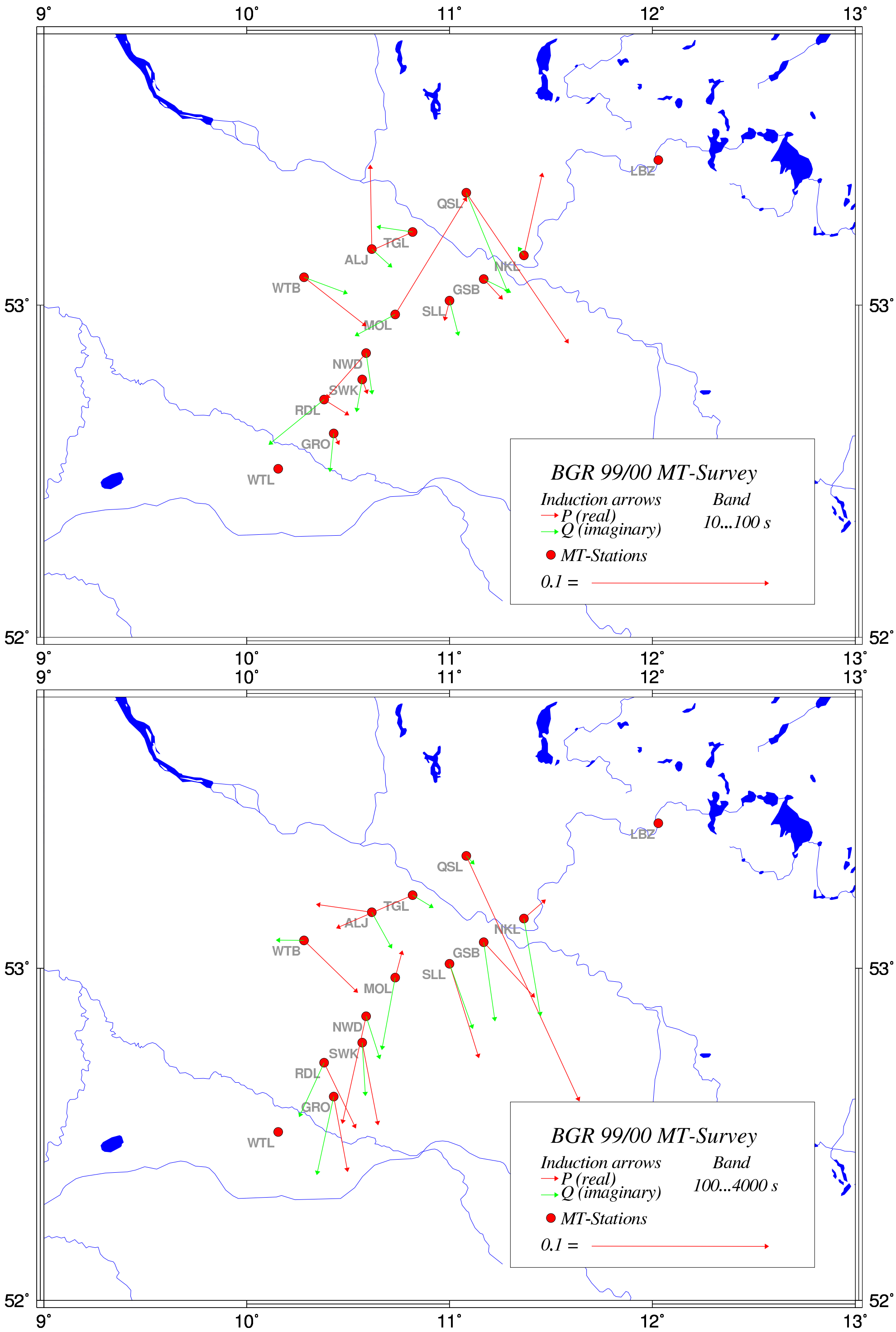

Figure A.8: Induction arrows, band averaged from 10 to 100 s and 100 s to 4000 Hz

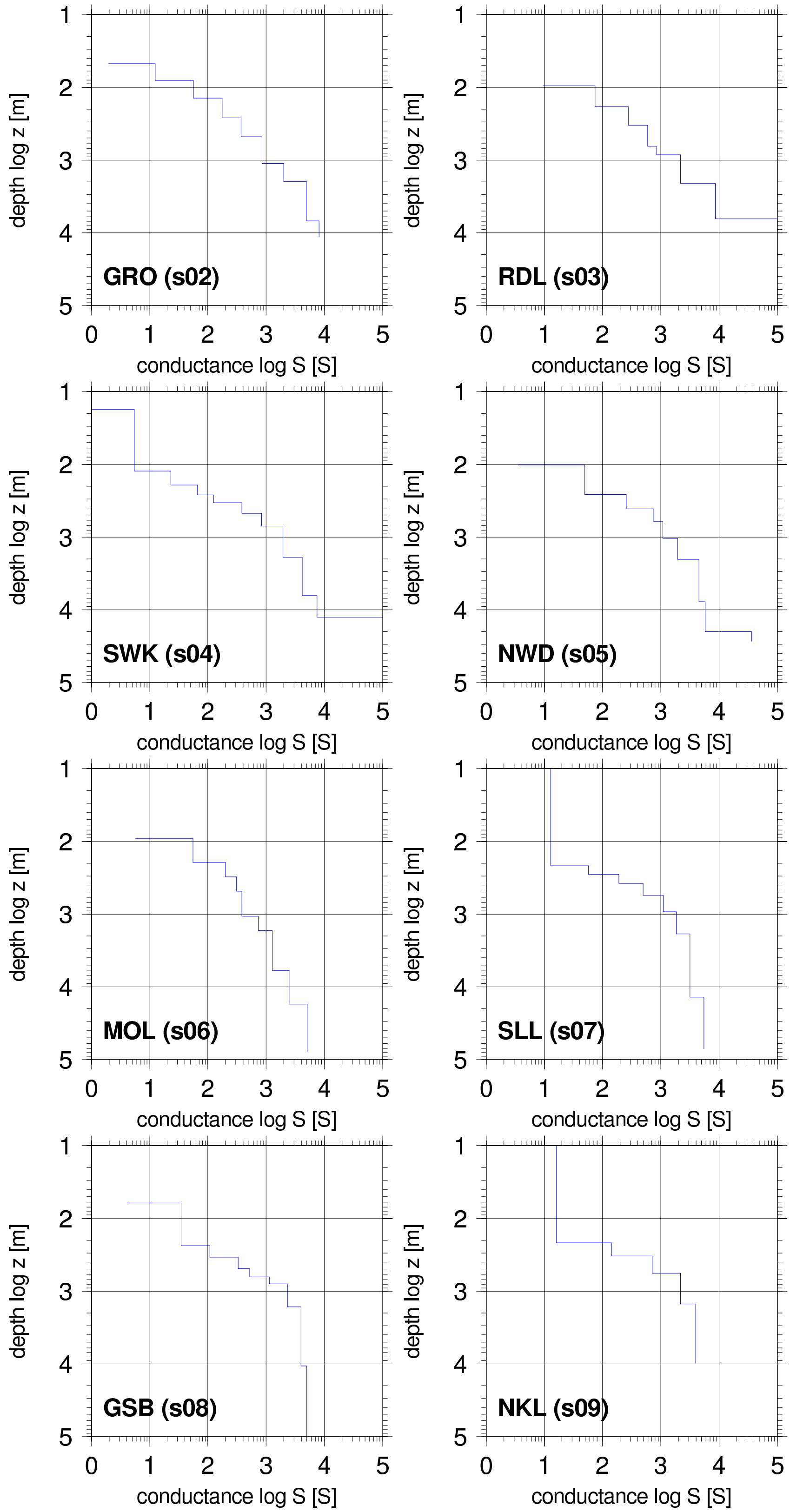

Figure A.9: 1D models derived from data of 300 Hz to 100 s, Line 1, stations 2 to 9

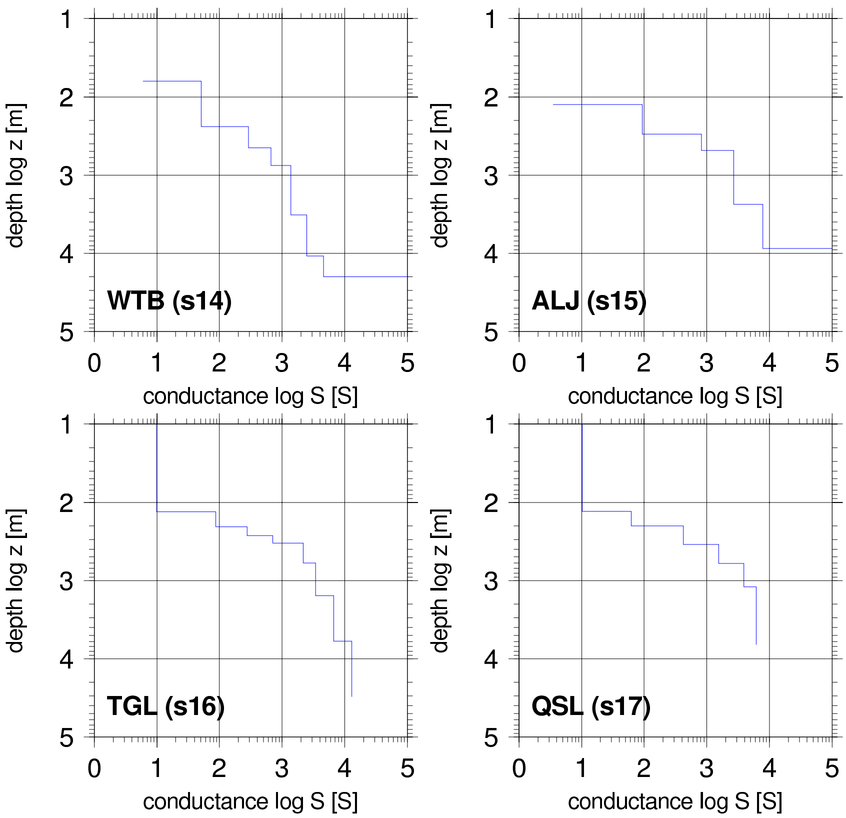

Figure A.10: 1D models derived from data of 300 Hz to 100 s, Line 2, stations 14 to 17

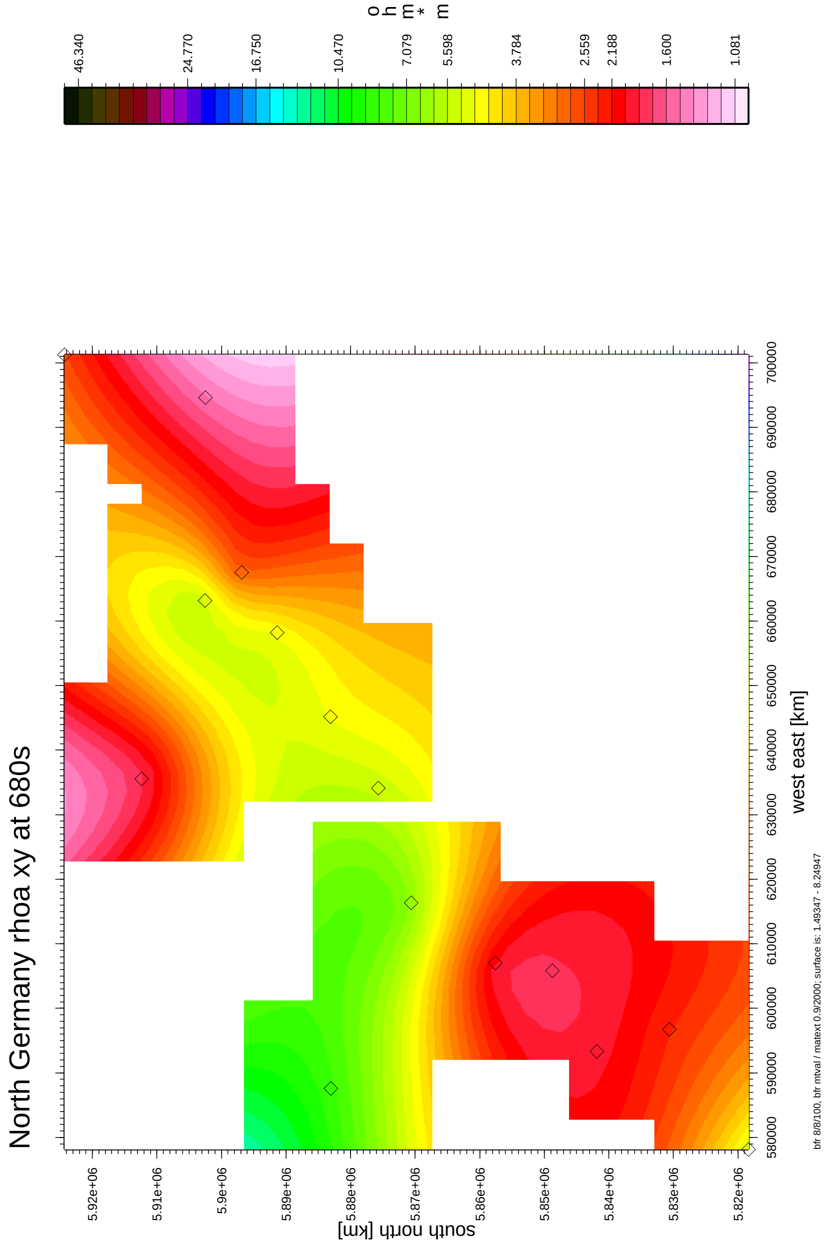

Figure A.11: Resistivity @ 670s, plan view

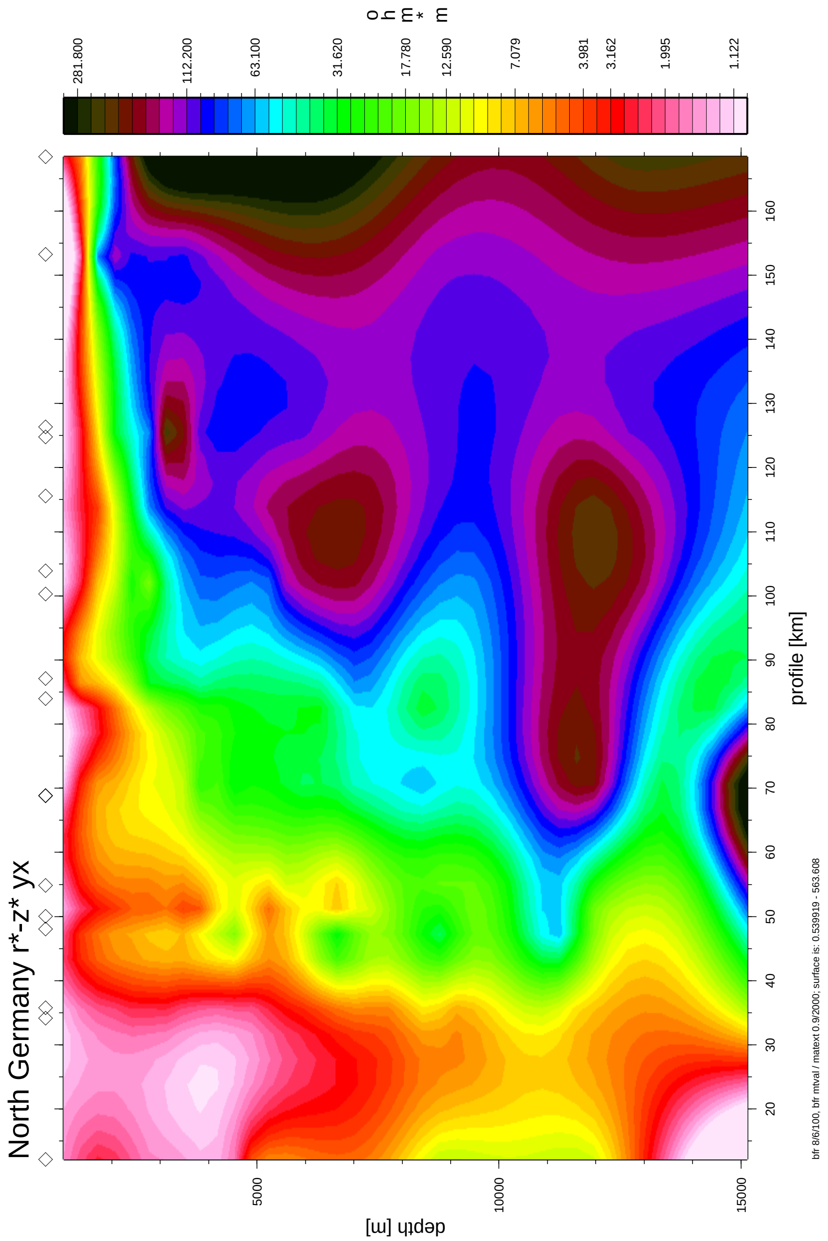

Figure A.12: r*-z* Cross Section along the profile

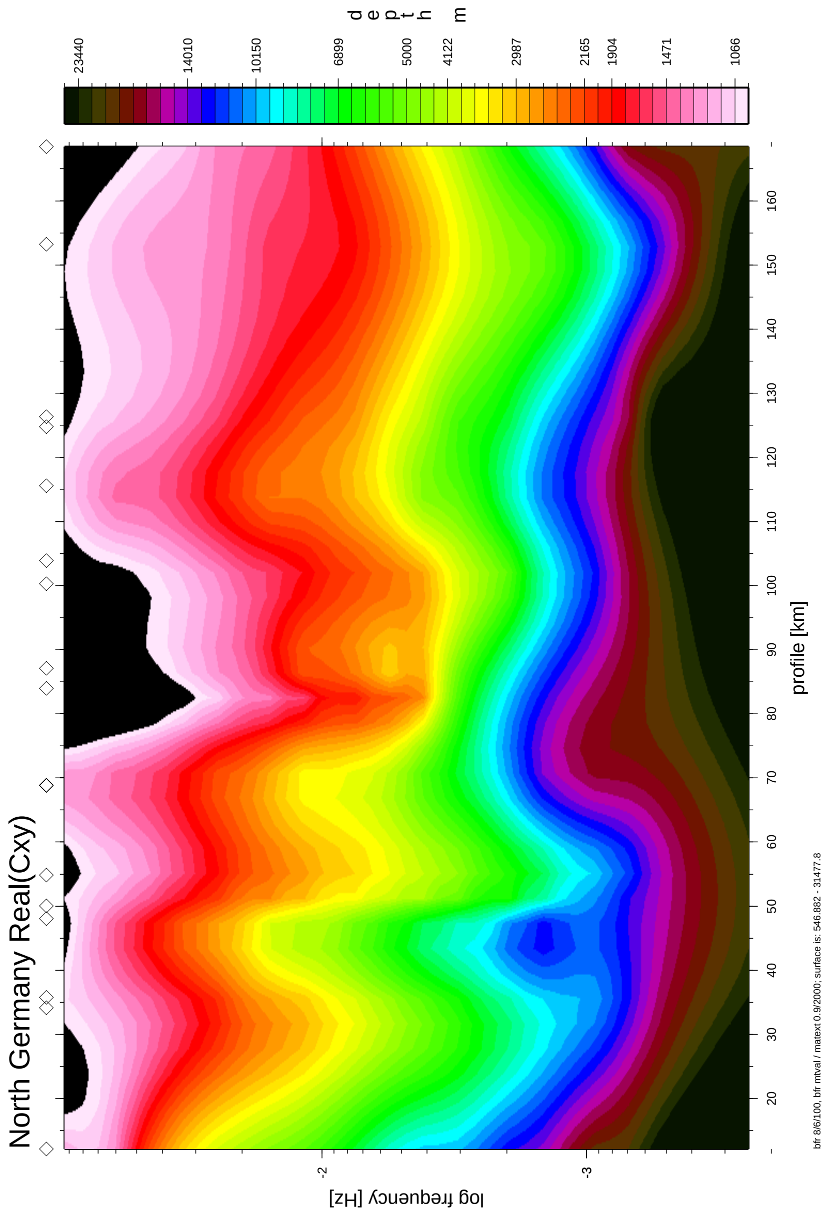

Figure A.13: Real Part of Schmucker's Cxy Transfer Function

Appendix B

Programs and used packages

During this thesis I wrote a lot of programs and scripts for converting data formats, generating data processing scriptsand data visualization scripts (GMT), etc. Most programs have been written in Perl (www.perl.org) and Fortran. Most software packages are summarized in Table B.1.

Software	Purpose	Source
AnalyzeMT	Robust code for MT data processing	Jimmy Larsen
GMT	Data visualization	http://www.soest.hawaii.edu/gmt/
MAPROS	Survey managment, processing	Metronix, Braunschweig
mtval	Deriving MT-values	B. Friedrichs
Perl	Writing scripts	http://www.perl.org
Fortran	Writing the fit algorithm	http://www.gnu.org

Table B.1: Used Software programs, packages and languages

List of Figures

List of Tables

Acknowledgements

At first I would like express my sincere thanks to Prof. Peter Weidelt for his very valuable support to this thesis.

Further I thank:
Jim Larsen for providing the time series processing code and his valuable and immediate support,

Bernhard Friedrichs for the chance to participate in this survey in place of the **metronix** team and for personal support and all advices,

Norbert Hoffmann (BGR) and Heinrich Brasse for additional pictures and information,

Kerstin Roden, Roland Schreiber, and Susanne Reichelt for proof-reading,

and all other members of the institute for their support, especially Kai Schweda and Andrea Diedrich for the good time.

Last but not least I want to express my sincere thanks to my family for their personal support and faith in me.